Nuclear Engineering Education Research Program
Project No. DE-FG07-04ID14598

An Innovative High Thermal Conductivity Fuel Design

Final Report
Period: 07/14/04 – 07/14/07

Submitted to the U.S. Department of Energy
October 14, 2007

PI: James S. Tulenko, tulenko@ufl.edu
Ph: (352) 392-1401 Fax (352) 392-3380
Co-PI: Ronald H. Baney, rbane@mse.ufl.edu

The University of Florida

College of Engineering
P.O. Box 118300
Gainesville, FL 32611-8300

Student Contributors to this report:

Jiwei Wang - Nuclear and Radiological Engineering Department

TABLE OF CONTENTS

LIST OF TABLES

Table page

LIST OF FIGURES

CHAPTER 1
INTRODUCTION

Uranium dioxide (UO_2) is the most common fuel material in commercial nuclear power reactors. UO_2 has the advantages of a high melting point, good high-temperature stability, good chemical compatibility with cladding and coolant, and resistance to radiation. The main disadvantage of UO_2 is its low thermal conductivity. During a reactor's operation, because the thermal conductivity of UO_2 is very low, for example, about 2.8 W/m-K at 1000 ^oC [1], there is a large temperature gradient in the UO_2 fuel pellet, causing a very high centerline temperature, and introducing thermal stresses, which lead to extensive fuel pellet cracking. These cracks will add to the release of fission product gases after high burnup. The high fuel operating temperature also increases the rate of fission gas release and the fuel pellet swelling caused by fission gases bubbles. The amount of fission gas release and fuel swelling limits the life time of UO_2 fuel in reactor. In addition, the high centerline temperature and large temperature gradient in the fuel pellet, leading to a large amount of stored heat, increase the Zircaloy cladding temperature in a lost of coolant accident (LOCA). The rate of Zircaloy-water reaction becomes significant at the temperature above 1200 ^oC [2]. The ZrO_2 layer generated on the surface of the Zircaloy cladding will affect the heat conduction, and will cause a Zircaloy cladding rupture.

The objective of this research is to increase the thermal conductivity of UO_2, while not affecting the neutronic property of UO_2 significantly. The concept to accomplish this goal is to incorporate another material with high thermal conductivity into the UO_2 pellet. Silicon carbide (SiC) is a good candidate, because the thermal conductivity of single crystal SiC is 60 times higher than that of UO_2 at room temperature and 30 times higher at 800 ^oC [3]. Silicon carbide also has the properties of low thermal neutron absorption cross section, high melting point, good chemical stability and good irradiation stability. Silicon carbide is expected to form a conductive

lattice in UO_2 for heat to flow out of the fuel pellet, and the thermal conductivity of SiC is anticipated to control the thermal conductivity of the fuel pellet.

In this research, the effect of the SiC additive on the neutronic properties of a UO_2 pellet was simulated by CASMO-3, a multi-group two-dimensional transport theory code. Three methods were studied to incorporate SiC into UO_2.

Firstly, silicon carbide whiskers were mixed with UO_2 particles and then hot press sintered to achieve dense pellets. Secondly, a polymer precursor, allylhydridopolycarbosilane (AHPCS), was used to generate a SiC coating on UO_2 particles prior to the hot press sintering process. Thirdly, chemical vapor deposition (CVD) process was used to coat UO_2 particles with a SiC layer prior to the sintering process. To avoid a reaction that occurs between UO_2 and SiC at 1377 ^{o}C [4], a two stages low temperature sintering method was used to sinter the mixture of SiC whiskers and UO_2 particles or the SiC coated UO_2 particles at 1200 ^{o}C. The sintered pellets were characterized by X-ray diffraction (XRD) and Scanning Electron Microscope (SEM), and the thermal conductivity of the sintered pellets was to be measured by laser flash method at Idaho National Laboratory. The centerline temperatures of the sintered pellets at the reactor operating condition were calculated based on the measured thermal conductivity.

CHAPTER 2
LITERATURE REVIEW

The Properties of Uranium Dioxide

The properties of uranium dioxide (UO_2) have been investigated for decades. UO_2 has a cubic fluorite (CaF_2) type crystal structure with a lattice parameter of 5.470Å at room temperature. The theoretical density of UO_2 is 10.96 g/cm3, and the melting point of UO_2 is 2865 ^oC. UO_2 also has the advantages of good high temperature stability, good chemical compatibility with cladding and coolant, and resistance to radiation.

The thermal conductivity is one of the most important properties of UO_2, because it determines the fuel temperature, thus directly affect the behavior and performance of fuel pellet in a reactor. Based on experiment data, Fink [1] recommended that the thermal conductive of 95% dense UO_2 can be calculated by Equation 2-1, which is plotted in Figure 2-1.

$$k = \frac{100}{7.5408 + 17.692t + 3.6142t^2} + \frac{6400}{t^{5/2}} \exp(\frac{-16.35}{t}) \qquad \text{Equation 2-1.}$$

where t = T (K)/1000, and k is the thermal conductivity of 95% dense UO_2 in W/m-K.

The thermal conductivity of UO_2 can be affected by the oxygen to uranium ratio. Uranium dioxide ($UO_{2.0}$) is easily oxidized in air. Uranium oxide with O/U ratio greater than 2.0 is called hyperstoichiometric UO_2; uranium oxide with O/U ratio less than 2.0 is called hypostoichiometric UO_2. The oxidation of UO_2 in air is a two-step reaction:

$$UO_2 \rightarrow U_3O_7/U_4O_9 \text{-} \rightarrow U_3O_8.$$

The intermediate oxidation products, U_4O_9 and U_3O_7, are derivatives of the fluorite structure in which clusters of interstitial oxygen atoms are centered on unoccupied cubic sites in the lattice, with accompanying displacement of neighboring U atoms [5]. U_3O_8 has an

orthorhombic lattice structure [6], and its density is 8.38 g/cm3, which is 24% less than UO_2. The density decrease results in an undesirable volume increase in the fuel.

The thermal conductivity of hyperstoichiometric UO_2 [7] is shown in Figure 2-2. The excess oxygen atoms act as phonon scattering centers, and reduce the thermal conductivity of UO_2. The thermal conductivity of hypostoichiometric UO_2 [8] is shown in Figure 2-3. The defects in the UO_2 crystal lattice also act as phonon scattering centers, and reduce the thermal conductivity of UO_2. In addition, hypostoichiometric UO_2 could contain uranium metal which could be highly reactive with other materials; hyperstoichiometric UO_2 may have an oxygen partial pressure sufficient to cause interaction with other materials [9]. The O/U ratio of an unknown $UO_{2.x}$ powder can be determined by measuring the weight difference of $UO_{2.x}$ and U_3O_8 oxidized by $UO_{2.x}$, or $UO_{2.x}$ and UO_2 reduced by $UO_{2.x}$ (for hyperstoichiometric UO_2).

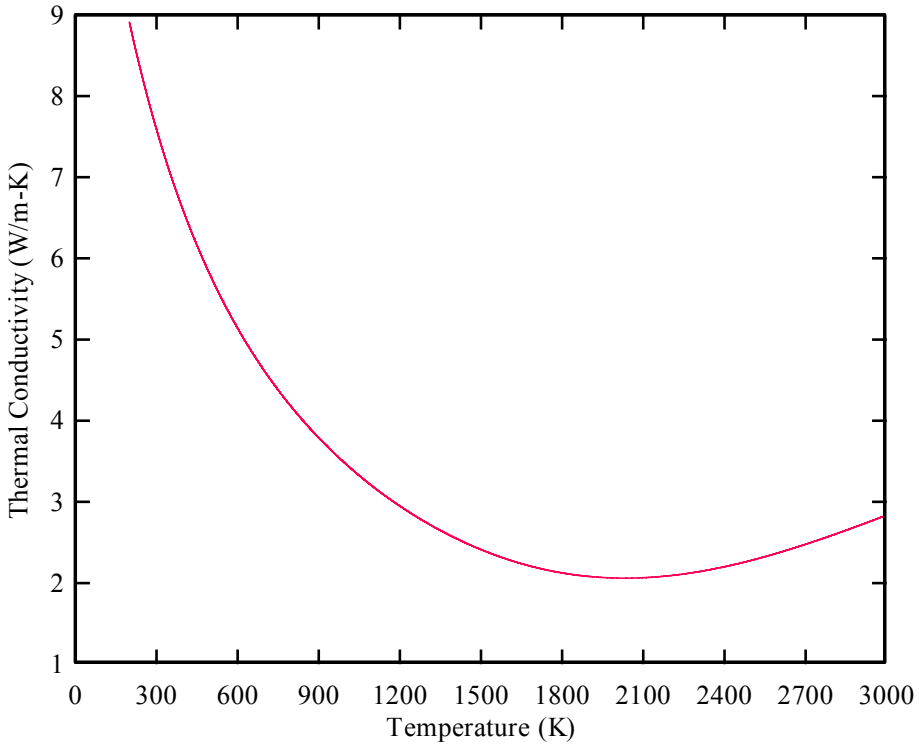

Figure 2-1. Thermal Conductivity of UO_2 versus Temperature.

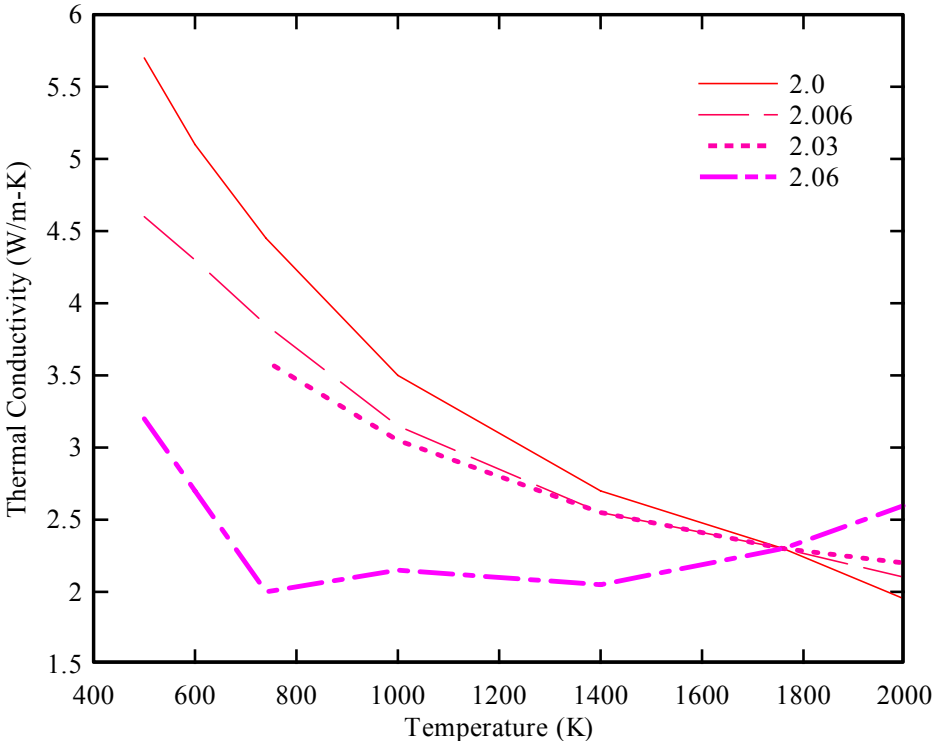

Figure 2-2. Thermal Conductivity of Hyperstoichiometric UO_2 versus Temperature.

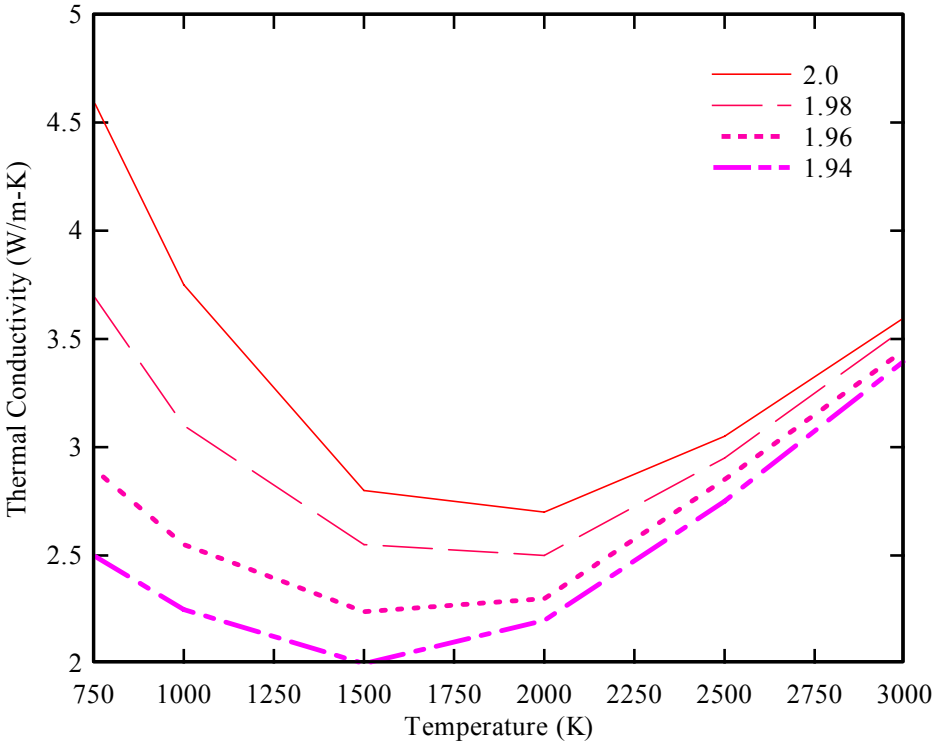

Figure 2-3. Thermal Conductivity of Hypostoichiometric UO_2 versus Temperature.

The thermal conductivity of irradiated UO_2 is affected by the changes that take place in the fuel during irradiation. During irradiation, fission products accumulate in the UO_2 matrix and cause fuel swelling. The fission products dissolved in the UO_2 lattice serve as phonon scattering centers, and reduce the thermal conductivity of the UO_2 fuel. Precipitated fission products have a much higher thermal conductivity of UO_2 and have a positive contribution to the thermal conductivity of UO_2 fuel. The fission product gases initially form in irradiated fuel as dispersed atoms within the UO_2 lattice, and then form small bubbles. The small bubbles within the UO_2 lattice also serve as phonon scattering centers, and reduce the thermal conductivity [10]. At temperature below 1000 ^oC, uranium dioxide retains essentially all the fission gases, but above this temperature the gases are released, and little fission gas remains in those region of the fuel where the temperature exceeds 1800 ^oC [11]. Radiation damage from neutrons, α-decay and fission products increase the number of lattice defects and consequently reduces the thermal conductivity of UO_2 fuel. The thermal conductivities of UO_2 before and after irradiation are shown in Figure 2-4. The radiation-induced decrease in the thermal conductivity of UO_2 is large at low temperature. Oxygen defects are known to anneal at around 500 K, and uranium defects largely anneal at 1000 K. This explains why most changes in the thermal conductivity of UO_2 are seen below 1000 K [10].

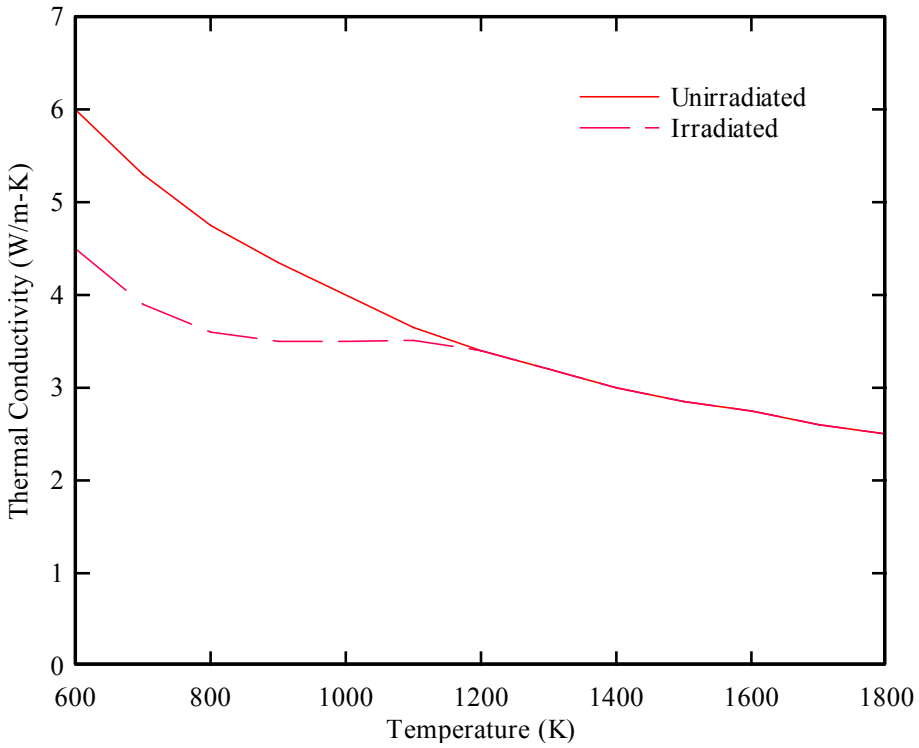

Figure 2-4. Thermal Conductivity of UO_2 before and after Irradiation.

The task of increasing the thermal conductivity of uranium dioxide (UO_2) has been sought for many years with little success. Si-Hyung Kim [12] reported a 50% increase in the thermal conductivity of UO_2 by adding 5 w% Mo at 1000 ^oC; however, Mo has a high thermal neutron absorption cross section. Ishimoto [13] reported a 25% increase in the thermal conductivity of UO_2 by adding 1.2 w% BeO; however, BeO is a very toxic material for handling. Solomon et al [14] has attempted to use silicon carbide (SiC) to increase the thermal conductivity of UO_2 by polymer infiltration pyrolysis (PIP) method; however, they failed to avoid the reaction between UO_2 and SiC at 1377 ^oC.

The Properties of Silicon Carbide

Silicon carbide (SiC) is a ceramic compound of silicon and carbon, and was discovered by Edward Goodrich Acheson around 1893. The basic block of the SiC crystal is the tetrahedron structure, and each silicon (Si) or carbon (C) atom is surrounded by four C or Si atoms. The

crystalline structure of SiC can be considered to consist of the close-packed stacking of double layers of Si and C atoms. The stacking of the double layers follows one of three possible relative positions. The positions are arbitrarily labeled A, B and C. The stacking sequences result in a large number of polytypes of SiC [15]. The only cubic form is β-SiC (3C-SiC), which has a stacking sequence of ABCABCABC. The density of SiC is in the range from 3.166 to 3.249 g/cm3 depending on the polytype [15].

Silicon carbide crystals can be manufactured by combining silica sand (SiO_2) and carbon at high temperature, between 1600 ^oC to 2500 ^oC. The purity of the SiC crystals produced is relatively low compared to the more expensive chemical vapor deposition (CVD) process. Chemical vapor deposition is a process of forming high purity solid materials using the decomposition/reaction of one or more gaseous precursors. Powell et al [16] used SiH_4 and propane to grow SiC on silicon substrate at 1360^oC. Nagasawa and Yamaguchi [17] have reported growth of 3C-SiC on Silicon substrate using SiH_2Cl_2 and C_2H_2 by low-pressure CVD. A single precursor containing both silicon and carbon can also be used in CVD process. Steckl et al. [18] have successfully investigated the growth of 3C-SiC on Silicon substrate using silacyclobutane (SCB) at temperatures as low as 800^oC. Kunstmann et al. [19] have reported the growth of 3C-SiC films using methyltrichlorosilane (Ch_3SiCl_3) at temperature around 1200 ^oC. Another method to produce crystalline silicon carbide is to use a polymer precursor. AllyHydridoPolyCarboSilane (AHPCS) was successfully converted to crystalline β-SiC at 1600 ^oC by Zheng et al [20].

The neutron capture cross-section for silicon carbide and comparative values for the fuel components are shown in Table 2-1. Both Si and C have a small thermal neutron absorption

cross section, so small amounts of SiC will not significantly affect the neutronic property of UO_2 fuel.

Table 2-1. Neutronic cross sections (barns).

	σ_{abs}(th)	σ_s(th)	σ_s(epi)
C	0.0032	4.8	4.66
Si	0.00019	4.2	3.7
O	0.13	5	3.4
Zr	0.18	8	6.2

One of the most attractive properties of SiC is its high thermal conductivity. The thermal conductivity of single crystal SiC measured by Slack at room temperature is 490 W/m-K [3], which is even higher than copper, at 398 W/m-K [21]. The thermal conductivity of polycrystalline β-SiC by CVD process is lower, about 70 W/m-K at room temperature [22]. Figure 2-5 shows the thermal conductivities of single crystal SiC and polycrystalline β-SiC versus temperature. The single crystal SiC has higher purity and less defects than the polycrystalline β-SiC. The boundaries in the polycrystalline β-SiC can also serve as phonon scattering centers. Figure 2-6 shows the thermal conductivity of polycrystalline β-SiC before and after irradiation [23]. The thermal conductivity of unirradiated SiC decreases with increasing temperature. The thermal conductivity of SiC is mainly controlled by the lattice vibration waves (Phonons). The phonon-phonon scatterings increase with increasing temperature, which decrease the phonon mean free path, and consequently decrease the thermal conductivity.

The thermal conductivity of SiC decreases by a factor between 3 and 9 at room temperature when SiC is irradiated with fast neutrons fluence of 2.7-7.7×10^{21} n/cm^2 (E>0.18 MeV) at 550 ^{o}C-1100 ^{o}C [23]. During fast neutron irradiation, point defects are introduced in the SiC lattice structure. These defects are the scattering centers for phonons, and thermal

conductivity is sharply reduced in consequence. The phonon mean free path is determined by the mean free path of defects, so the thermal conductivity is almost independent of temperature after irradiation.

Amorphous SiC was observed by Snead [24] using transmission electron microscopy (TEM) after irradiation of β-SiC with fast neutron of 2.6×10^{25} n/m^2 (E>0.1 MeV) at 53 ^{o}C. The thermal conductivity of amorphous SiC is only 5.4 W/m-K at 800 ^{o}C, only slightly higher than UO_2. The annealing effect was also observed by Snead. The SiC crystallites grow slowly in the ~800-1100 ^{o}C temperature range and the crystallite growth rate is approximately linear with annealing temperature; the SiC crystallites grow rapidly in the temperature range of 1100-1150 ^{o}C, with both faster growth of the existing crystallites and rapid nucleation of new crystallites throughout the amorphous material. No amorphous SiC is found after annealing at 1150 ^{o}C for 30 min [24].

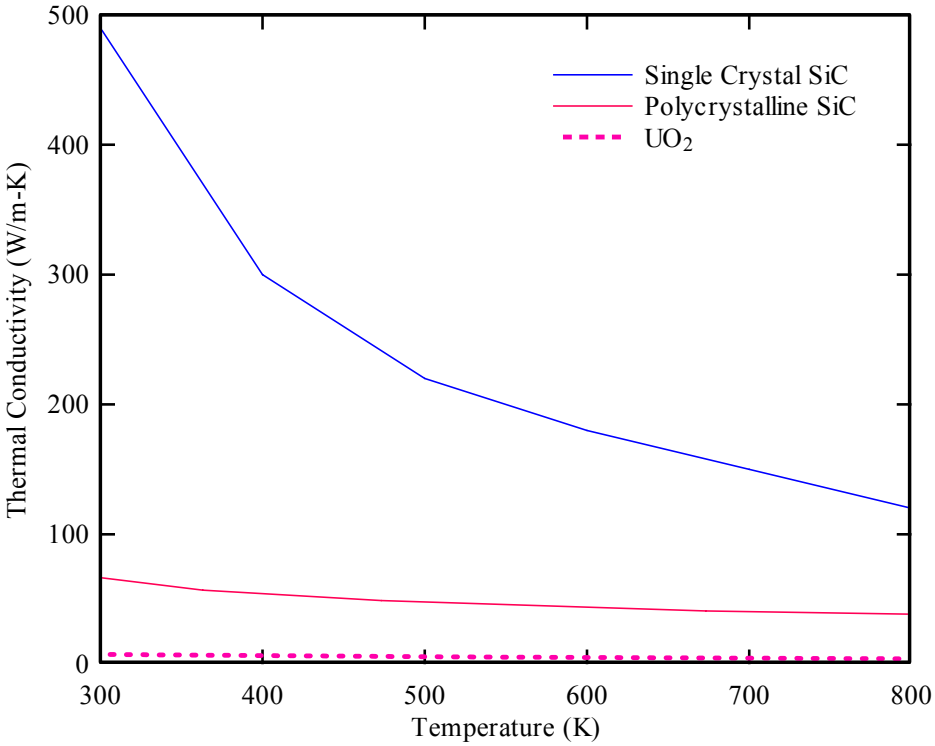

Figure 2-5. Thermal Conductivity of Single Crystal SiC and Polycrystalline SiC.

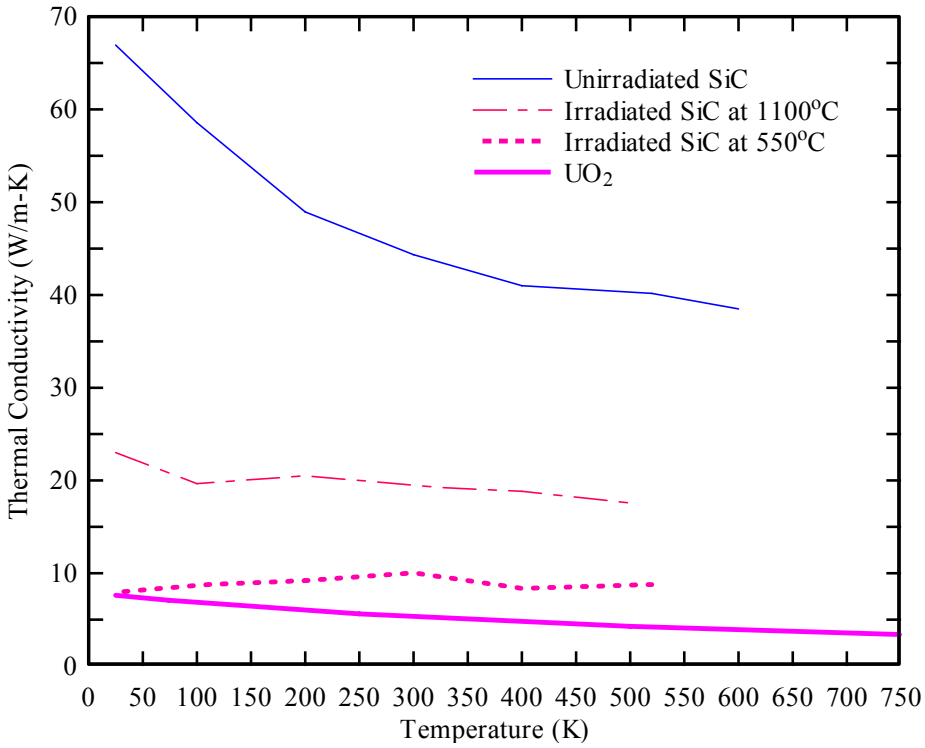

Figure 2-6. Thermal Conductivity of β-SiC Before and After Irradiation.

Silicon carbide is chemical inert which is aided by the silicon oxide (SiO_2) layer formed on it. Silicon carbide is not attacked by any acids or alkalis or molten salts at room temperature. Verral reported that the SiC lost 2% at 573 K in deoxygenated water of pH 10.3 after 90 days, and less than 2% at 573K in deoxygenated water of pH 3 after 32 days [25]. Hirayama also reported the weight loss increased with increasing pH value, the weight loss in the oxygenated solution was more than that in the deoxygenated solution [26]. Verral reported that there was no significant interaction between SiC and Zircaloy-4 at 1273 K; at 1773 K there was a diffusion-based reaction to form ZrC and free SiC, but the SiC Zircaloy cladding interaction was no worse than the UO_2-Zircaloy cladding interaction [25].

Silicon carbide materials have been widely used as the inert matrix material for Gas Cooled reactors. In that use, SiC has shown the capability to maintain its properties under high irradiation and temperature conditions. There is a slightly expansion at fluences up to

5×10^{26}n/m2 and irradiation temperature below 1000 ^{o}C. At higher temperature, irradiation creates voids that cause continuing expansion, but the structural integrity is not affected. The irradiation has a negligible effect on the strength of SiC [22].

Silicon carbide is used for furnace parts because of its high melting point. The unique properties of SiC, such as wide band gap, high saturated electron drift velocity, high thermal conductivity, high breakdown electric field, make it a promising semiconductor for high temperature, high power, and high speed usages.

Reaction between Uranium Dioxide and Silicon Carbide

There are very few papers are about the reaction between uranium dioxide (UO_2) and silicon carbide (SiC). A study by G. C Allen et al [4] had shown that UO_2 reacts with SiC at a measurable rate above 1377 ^{o}C. The possible reaction equations are as follows:

$UO_2 + 2SiC \leftrightarrow USi_2 + 2CO$ Equation 2-2

$UO_2 + 2SiC \leftrightarrow UC_2 + 2SiO$ Equation 2-3

$USi_2 \leftrightarrow USi_{1.67} + 0.33Si$ Equation 2-4

$5Si + 3UC_2 \leftrightarrow U_3C_3Si_2 + 3SiC$ Equation 2-5

$UO_2 + 3UC_2 \leftrightarrow 4UC + 2CO$ Equation 2-6

W. Lippmann et al [27] confirmed the reaction between UO_2 and SiC at a temperature above 1700 ^{o}C in a system where gaseous products were free to escape. However, they also found that there was not a reaction up to 1800 ^{o}C in a system where gaseous products were sealed. Solomon et al [28] also observed reactions between UO_2 and SiC above 1350 ^{o}C. The scanning electron microscope (SEM) image of the reaction at 1400 ^{o}C after 15h is shown in Figure 2-7.

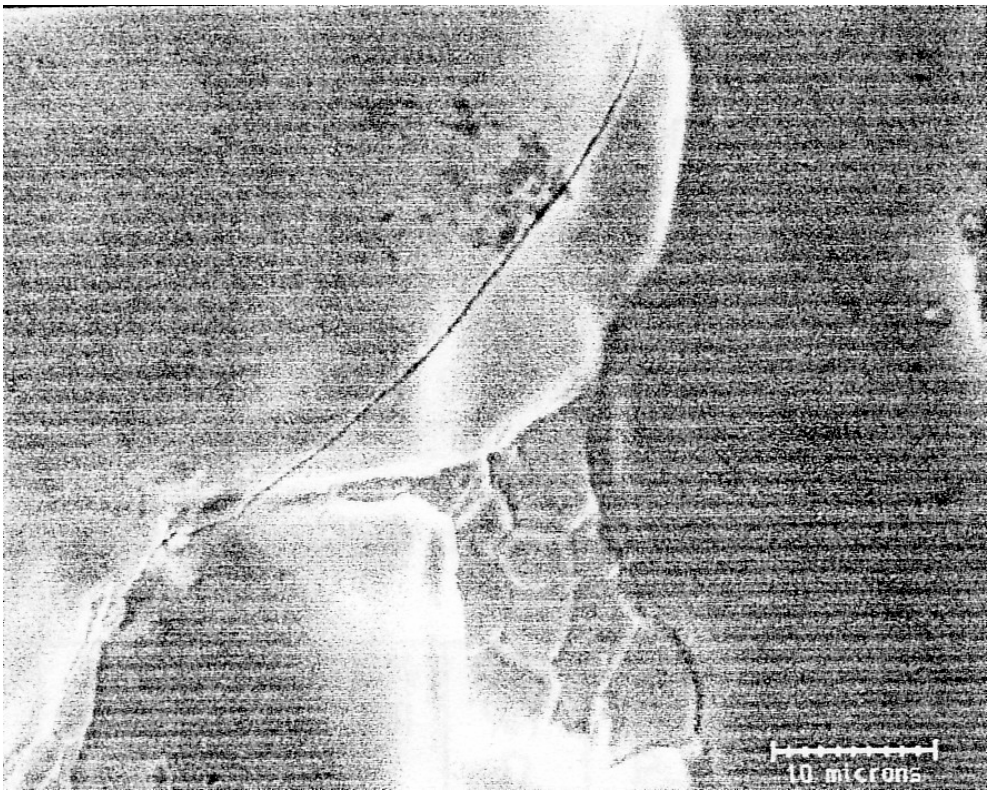

Figure 2-7. SEM image of UO_2 and SiC reaction at 1400 ^oC.

Low Temperature Sintering of Uranium Dioxide

Uranium dioxide (UO_2) pellets are normally made by sintering green UO_2 pellets at about 1700 ^oC in a hydrogen containing gas atmosphere. The high sintering temperature is necessary to achieve the required high density of over 95% of theoretical. However, sintering at a temperature around 1700 ^oC is expensive due to energy cost and furnace maintenance cost.

Several studies have shown that UO_2 pellets with the required high density can be achieved at lower sintering temperature. Fuhrman et al [29] reported that UO_2 pellets of 95 to 97% theoretical density (TD) were attained by sintering at 1200 ^oC in nitrogen for 1 hour, followed by 1 hour reduction in hydrogen, using uranium oxide powder with extra oxygen (O/U ~ 2.37). They also mentioned that UO_2 pellets of 95% TD were achieved at a temperature as low as 1000

^{o}C using the same method, though the result was not consistent. Langrod [30] sintered UO_2 pellets to densities above 95% TD with temperatures at 1300 ^{o}C using an argon or nitrogen atmosphere for 2 hours followed by reduction in hydrogen, with a mixture of UO_2 and U_3O_8 (O/U ~ 2.30). Ayaz et al [31] sintered UO_2 pellets to 95% TD at temperatures of 1150 ^{o}C in CO_2 and water vapor atmosphere for 4 hours, followed by reduction in Ar+8% H_2 for 1hour, using uranium oxide powder with extra oxygen (O/U = 2.15). Williams et al [32] studied sintering uranium oxide with different O/U ratio in argon, nitrogen, carbon dioxide and vacuum, and achieved UO_2 pellets of 94% TD at temperatures lower than 1400 ^{o}C in various gases.

Excess oxygen was believed to be the key factor needed to decrease the sintering temperature. In the sintering process, the uranium oxide particles undergo solid state diffusion. Based on the theory by Williams et al [32], the rate of the diffusion of uranium ions determines the rate of the sintering process, and the diffusion of uranium ions in non-stoichiometric uranium oxides is more rapid than in stoichiometric UO_2 because the extra oxygen in non-stoichiometric uranium oxides lowers the lattice binding energies.

To increase the oxygen to uranium ratio, the uranium oxide powder was oxidized in air. The rate and degree of oxidation of UO_2 versus temperature was studied by Langrod [30], as shown in Figure 2-8. Langrod also found that the sintering behavior of UO_2 powder blended with U_3O_8 was identical with the air oxidized UO_2 powder of the same O/U ratio [30].

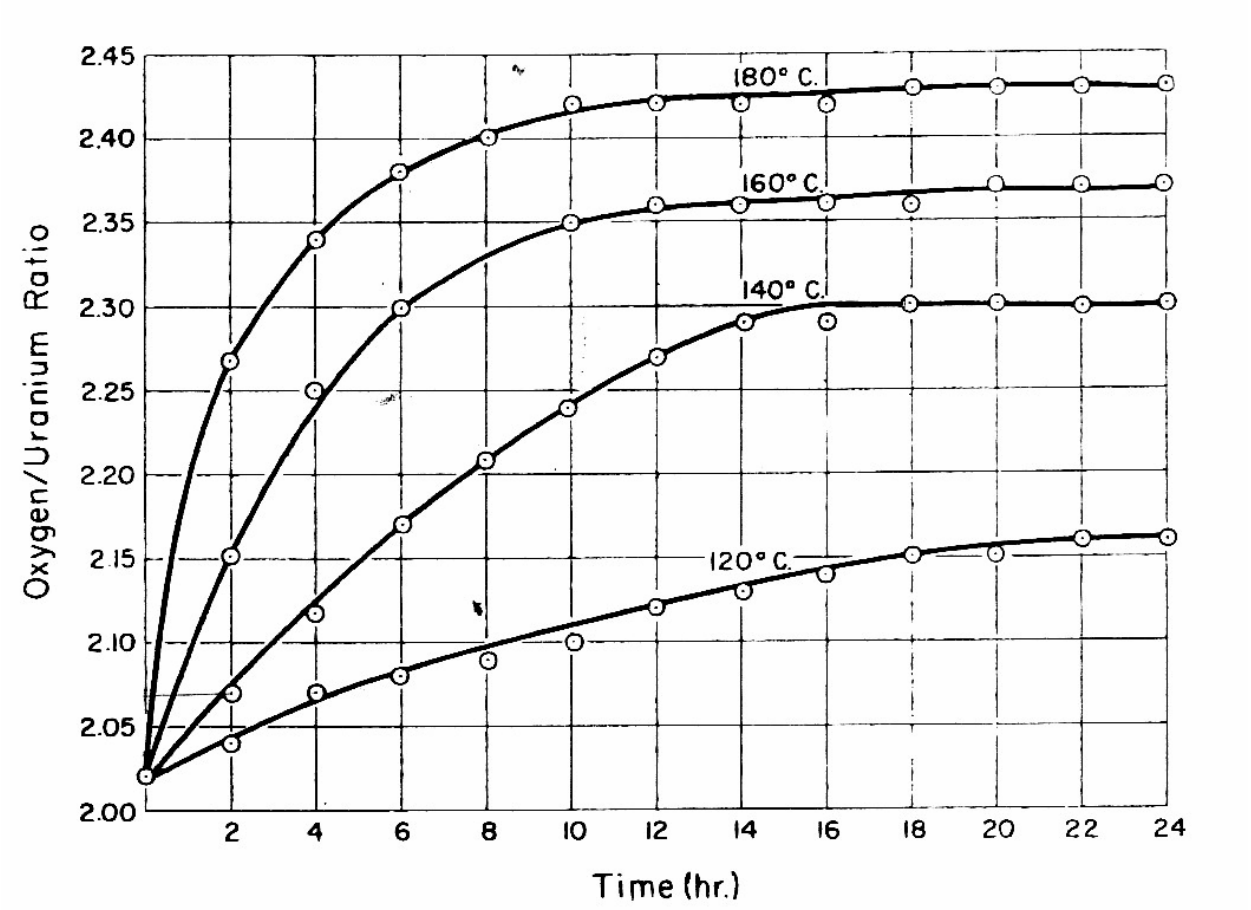

Figure 2-8. Oxidation of UO_2 in Air versus Temperature.

The study by Fuhrman et al [29] showed that the micro structure of low temperature sintering is smaller than the grain size of high temperature sintered pellets, as shown in Figure 2-9. A larger grain size is preferred for UO_2 pellet to minimize the fission gas release.

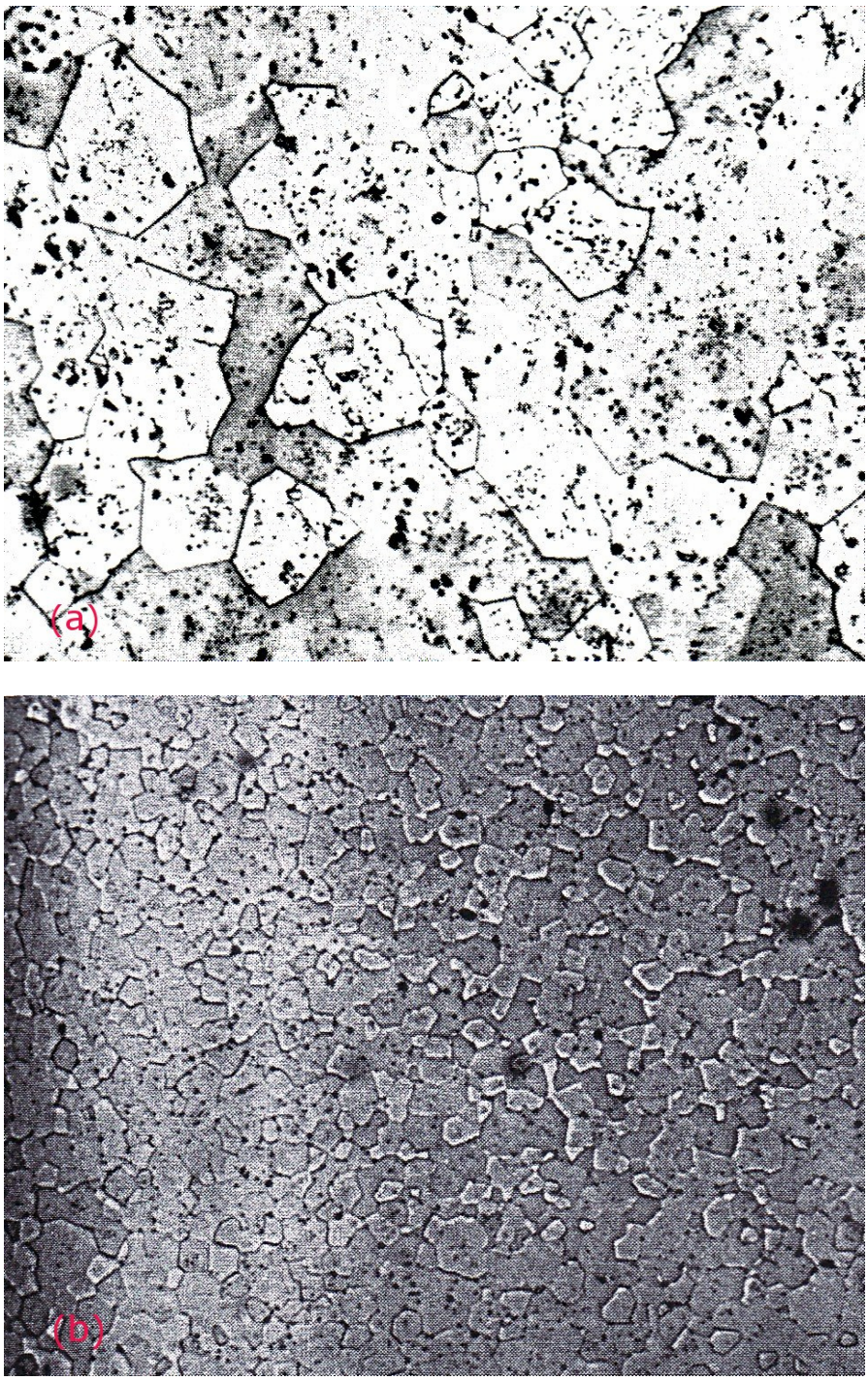

Figure 2-9. Microstructure of the Sintered UO_2 Pellets. (a), UO_2 PelletSintered at 1650 ^oC for 6 hours in H_2. (X250) (b), UO_2 Pellet Sintered at 1300 ^oC for 1 hour N_2, 1 hour in H_2. (X250)

The non-stoichiometric pellets must be further processed to bring the oxygen to uranium ratio back to 2.0 by soaking the pellets in a hydrogen environment. Fuhrman et al [29] reported that 1100 ^{o}C was required to remove the excess oxygen in a reasonable time.

Silicon Carbide Whisker Reinforced Ceramics

Silicon carbide (SiC) whiskers are usually used as a reinforcing material to improve the mechanical properties, such as strength and fracture toughness, of matrix materials. Wei et al [33] used SiC whiskers to reinforce aluminum oxide (Al_2O_3) to improve the fracture toughness. Sun et al [34] used SiC whiskers to improve the fracture toughness and high temperature strength of molybdenum disilicide ($MoSi_2$). The mechanisms of strengthening and toughening relevant to whisker reinforcement are matrix pre-stressing, micro-cracking and whisker pull out.

Silicon carbide whiskers are commonly made by either the rice hull [35] or vapor-liquid-solid (VLS) [36] process. The SiC whiskers produced from the rice hull process are typically less than 1 micron in diameter and range from 10 to 50 micron in length. The SiC whiskers produced from VLS process are typically 5-6 micron in diameter and up to 100 mm in length [37]. Silicon carbide whiskers are single crystal, which means fewer flaws than polycrystalline, so the strengths and Young's module are very high.

The commercially available SiC whiskers are commonly in an agglomerated form. The agglomeration must be broken before being mixed with the matrix to ensure a homogenous dispersion of SiC whiskers. Wei et al [33] reported that SiC whiskers and ceramic powder were mixed in hexane in a blender and then dispersed using an ultrasonic homogenizer. The hexane was then dried by evaporation with constant agitation under flowing air.

To achieve a high density pellet, hot pressing is usually required because the whiskers interfere with matrix particle rearrangement during sintering. During hot pressing, SiC whiskers

are preferentially oriented in a plane perpendicular to the hot pressing axis. The optical images (Figure 2-10), taken by Hasselman et al [38], show the SiC whiskers alignment difference in the direction parallel and normal to the hot pressing direction.

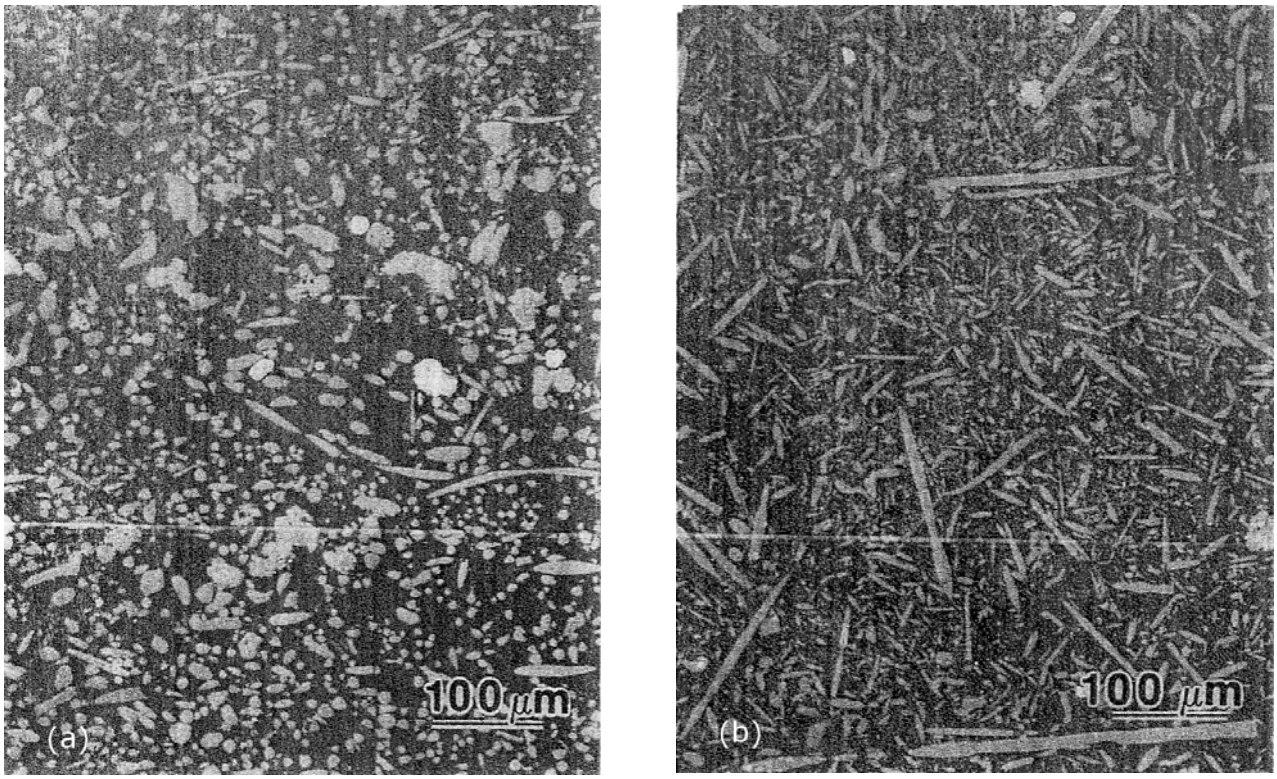

Figure 2-10. Optical micrographs of a 30 vol% VLS SiC whisker-reinforced lithium aluminosilicate glass. (a), parallel to hot pressing direction. (b), normal to hot pressing direction.

Several studies have shown that SiC whiskers can also increase the thermal conductivity of matrix materials. Russell et al [39] reported the thermal conductivity of 30 vol% VLS SiC whisker-mullite composite is three times higher at room temperature than that of the single phase mullite in the direction perpendicular to the hot pressing direction, and two times higher in the parallel direction. Johnson et al [40] reported that the thermal conductivity of a 30 vol% SiC whisker-osumilite glass composite is four times higher at room temperature than that of single phase mullite in the direction perpendicular to the hot pressing direction, and two times higher in the parallel direction, as shown in Figure 2-11. Hesselman et al [38] showed the thermal

conductivity of 30 vol% VLS SiC whisker-lithium aluminosilicate glass composite is five times higher at room temperature than that of lithium aluminosilicate glass in the direction perpendicular to the hot pressing direction, and three times higher in the parallel direction. Hesselman et al suggested that a SiC whisker "percolation" pathway was formed, and that the heat was conducted through the SiC whiskers, bypassing the matrix.

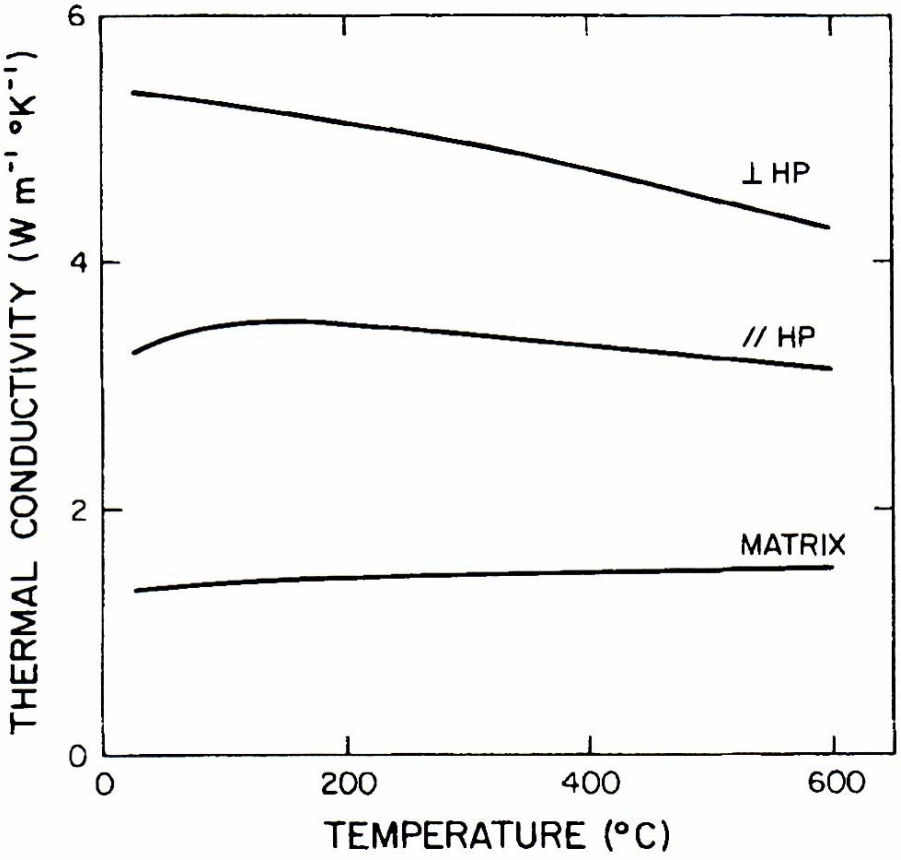

Figure 2-11. Effect of Silicon Carbide Whisker on the Thermal Conductivity of Osumilite Glass Ceramic.

CHAPTER 3
ANALYSIS, EXPERIMENT AND RESULTS

Neutronic Calculation

CASMO-3, a multi-group two-dimensional transport theory code, was used to study the effects of silicon carbide (SiC) on the reactivity of uranium dioxide (UO_2) fuel. The simulation utilized a Framatome Mark-B 15X15 assembly design. The power of the assembly is 14.37 MW. There are 208 fuel rods, 16 guide tubes and 1 instrument tube per assembly. The cross section view of Mark-B assembly is shown in Figure 3-1.

The reactivity of UO_2 fuel and the reactivity of UO_2 with 5 w%, 10 w% and 20 w% SiC versus burnup is shown in Table 3-1 and Figure 3-2. The reactivity of UO_2 fuel is less than the reactivity of UO_2 with 5 w%, 10 w% and 20 w% SiC at the beginning of life (BOL) because SiC replaces uranium 238, which has a large resonance absorption cross section, and the carbon atoms provide additional moderation. More neutrons slow down to the thermal region. As the fuel burns up, the reactivity of UO_2 decreases slower than the reactivity of UO_2 with 5 w%, 10 w% and 20 w% SiC because the thermal utilization factor, the ratio of the number of thermal neutrons absorbed in the fuel to the number of thermal neutrons absorbed in any materials, in UO_2 with SiC whiskers is decreasing faster than in UO_2 fuel. At the end of life (EOL), 60 MWd/KgU, the reactivity of UO_2 with 5 w% SiC, 10 w% SiC and 20 w% SiC is about 8%, 16% and 27% less than the reactivity of UO_2 fuel.

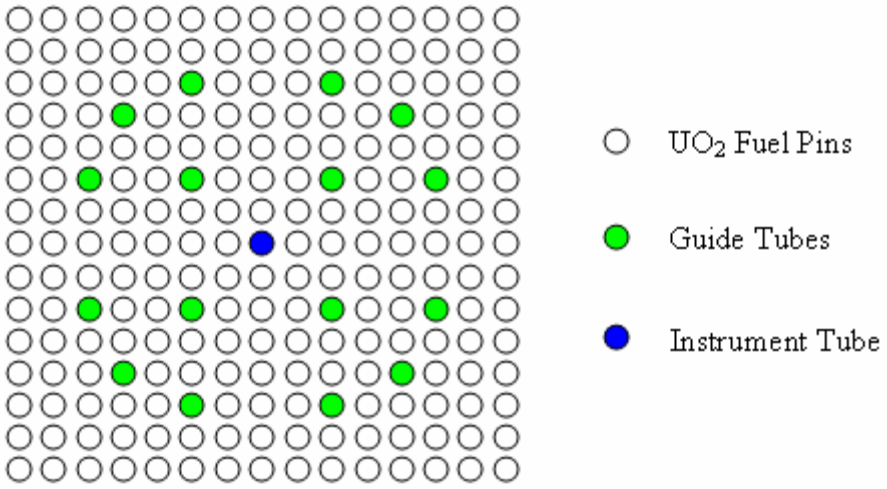

Figure 3-1. Crystal River 15X15 Assembly Design

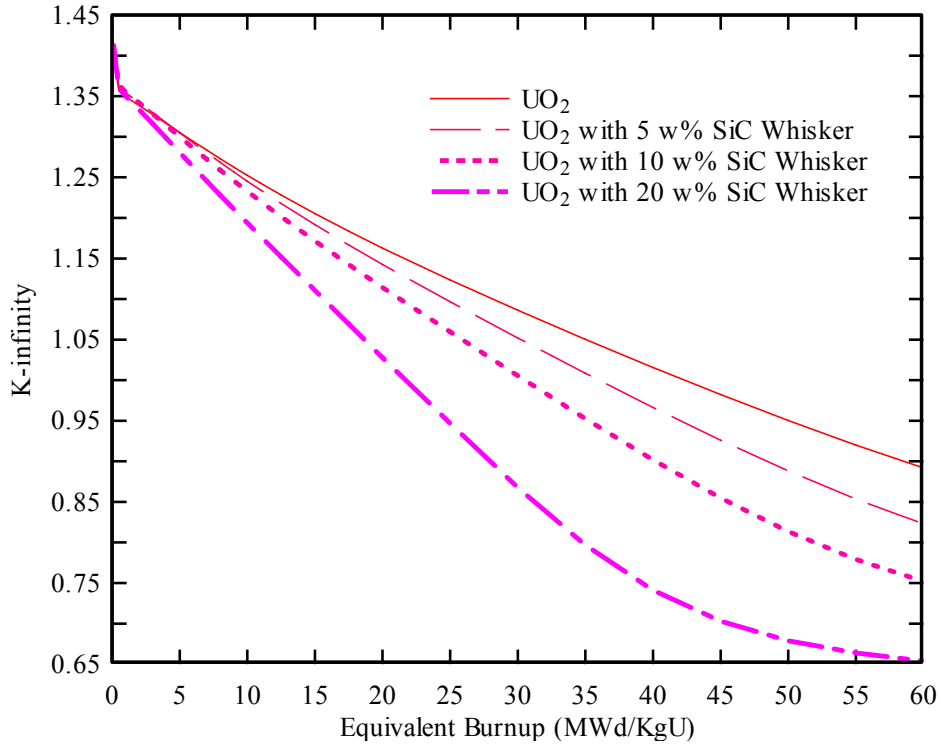

Figure 3-2. K-infinity Versus Burnup for UO_2 and UO_2 with Different Amounts of SiC

Table 3-1. K-infinity Versus Burnup for UO_2 and UO_2 with Different Amounts of SiC.

Equivalent Burnup (MWd/KgU)	UO_2	UO_2 with 5 w% SiC	UO_2 with 10 w% SiC	UO_2 with 20 w% SiC
0	1.4105	1.41914	1.42516	1.42834
5	1.30534	1.30491	1.30005	1.28053
10	1.25243	1.24523	1.23279	1.19385
20	1.16272	1.14256	1.1142	1.02764
30	1.08612	1.052	1.00548	0.86774
40	1.01558	0.96635	0.90176	0.74117
50	0.95029	0.88815	0.81343	0.67893
60	0.89182	0.8228	0.75196	0.65381

Characterization of the Uranium Oxide Powder

O/U Ratio

To measure the O/U ratio of the received uranium oxide powder from Framatome/Areva, the powder was oxidized to U_3O_8 and the weight difference was measured. The powder was oxidized in air at 350 ^oC for 24 hours. The weight change indicated the O/U ratio of received uranium oxide powder was 2.10. The generated U_3O_8 was reduced to $UO_{2.0}$ in a hydrogen environment at 900 ^oC for 4 hours. The received uranium oxide powder was oxidized in air at 140 ^oC for 24 hours, and the O/U ratio calculated by weight difference was 2.27.

Figure 3-3 shows the uranium oxide powder with different O/U ratio. The received $UO_{2.10}$ powder was dark brown; the $UO_{2.27}$ was black; the U_3O_8 powder was dark green; and the $UO_{2.0}$ powder was orange. The X-ray diffraction (XRD) results of the four uranium oxide powders were shown in Figure 3-4 to Figure 3-7. The XRD peaks of $UO_{2.0}$ were close to the peaks of $UO_{2.10}$ and $UO_{2.27}$, the extra oxygen in $UO_{2.10}$ and $UO_{2.27}$ slightly broadens and offsets the peaks of $UO_{2.0}$. The XRD peaks of U_3O_8 were totally different from the peaks of $UO_{2.0}$ because the crystal structures were different.

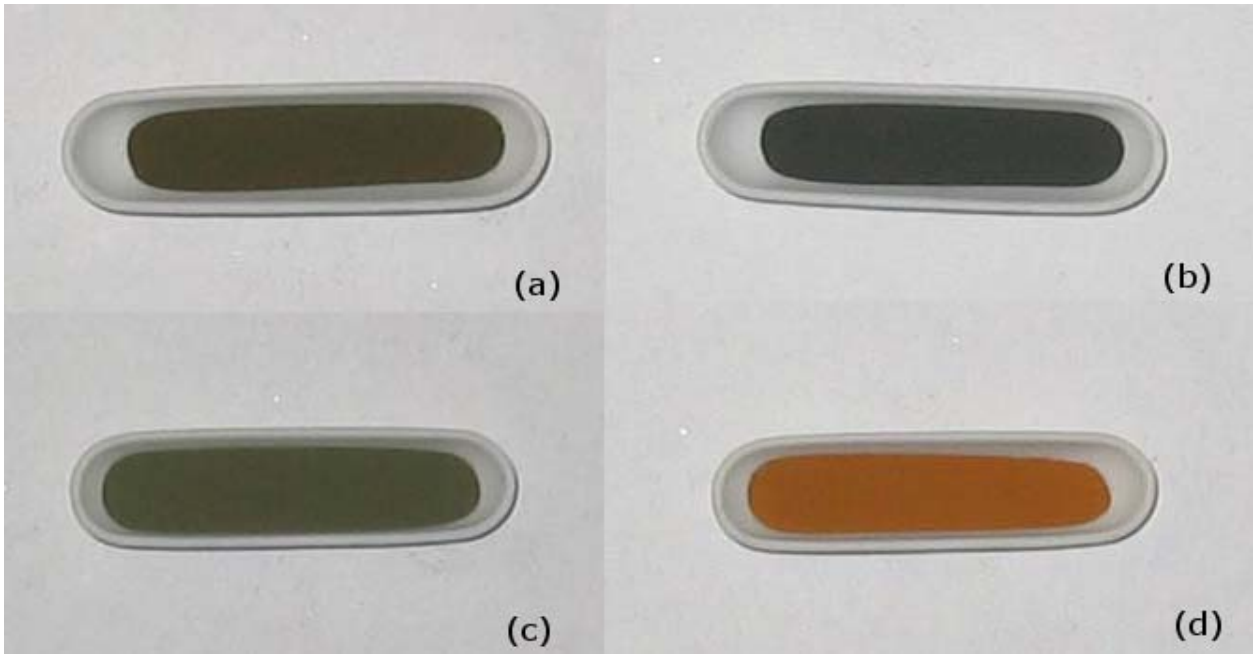

Figure 3-3. Uranium Oxide Powders with Different O/U Ratio (a), $UO_{2.10}$ (b), $UO_{2.27}$ (c), U_3O_8 (d), UO_2

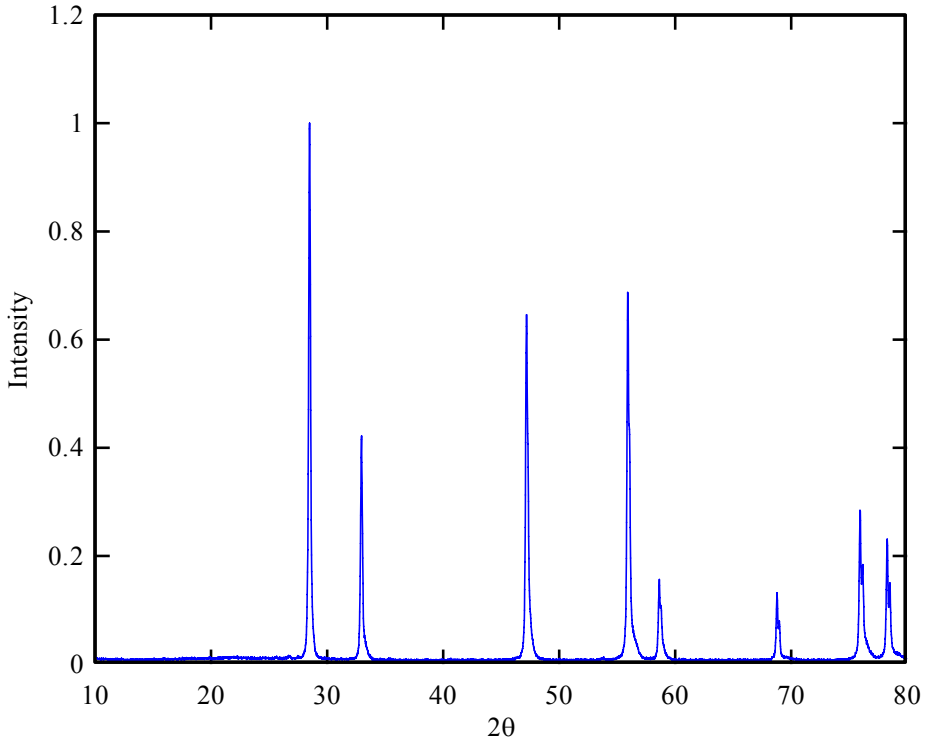

Figure 3-4 X-ray diffraction pattern of received $UO_{2.10}$ powder

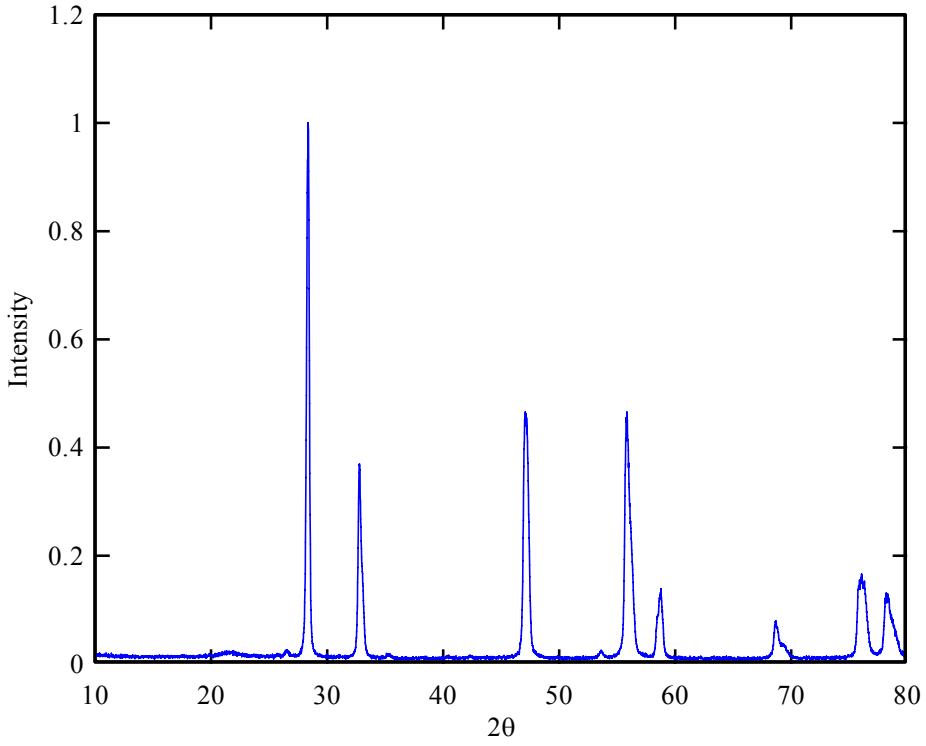

Figure 3-5. X-ray Diffraction Pattern of $UO_{2.27}$ Powder.

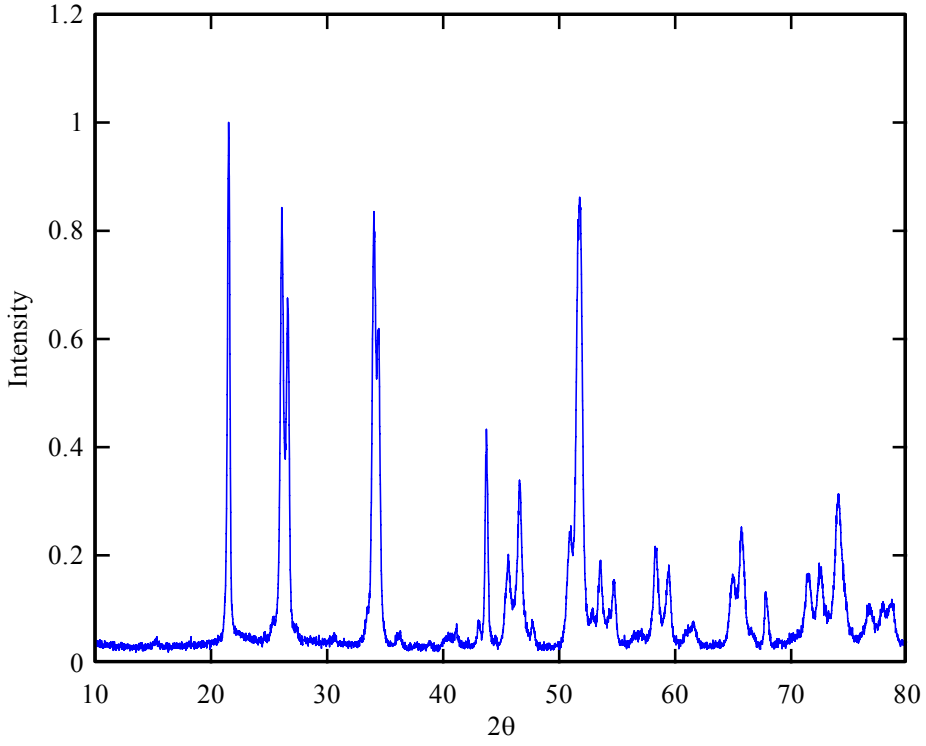

Figure 3-6. X-ray Diffraction Pattern of U_3O_8 Powder.

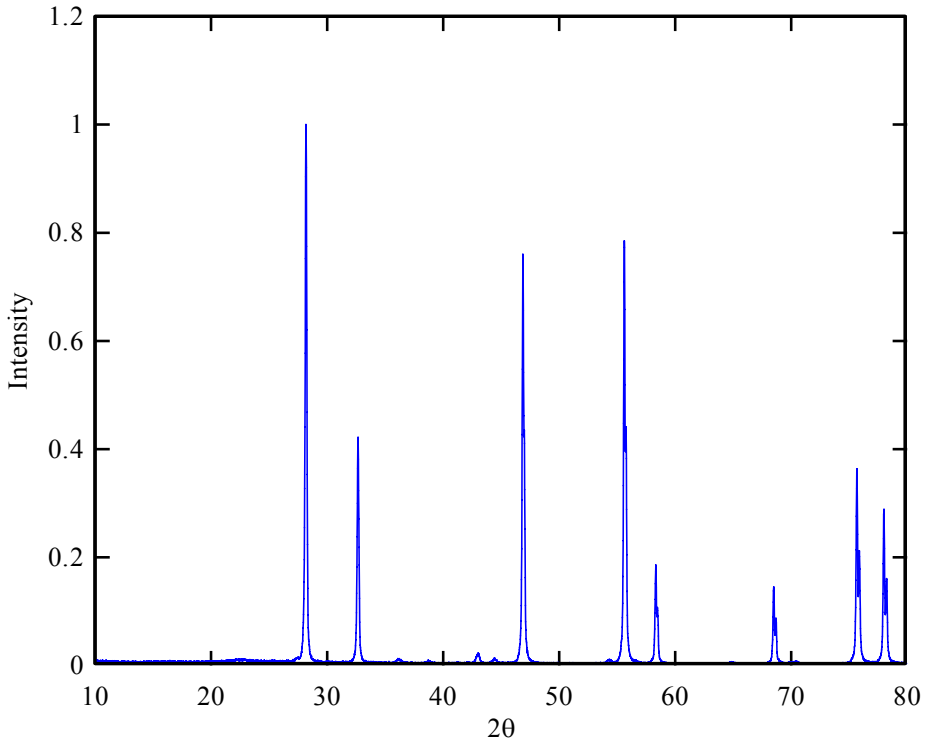

Figure 3-7. X-ray Diffraction Pattern of $UO_{2.0}$ Powder.

Particle Size Distribution

The particle size of the received $UO_{2.10}$ powder was characterized by a sieve analysis. The $UO_{2.10}$ powder was sieved through a series of screens with standardized mesh size. The sieve was put on an Octagon digital sieve shaker, and was shaken for half an hour. The sieve and shaker are shown in Figure 3-8. The powder between the two screens was weighed and recorded in Table 3-3. The experiment was repeated three times, and the average value was plotted in Figure 3-9.

.

Figure 3-8. Sieve and Shaker for Analyzing Particle Size Distribution.

Table 3-2. Particle Size Distribution of Received $UO_{2.10}$ Powder.

Particle Size (μm)	Weight (g)	Weight (g)	Weight (g)	Average (g)
<25	0.6767	0.5633	0.6769	0.6390
>25 and < 45	1.9094	1.9317	1.9308	1.9240
>45 and <53	1.0295	1.1097	1.0454	1.0615
>53 and <63	0.8636	0.8886	0.9009	0.8844
>63 and <90	2.4028	2.4171	2.3799	2.3999
>90 and <150	1.4126	1.4529	1.4846	1.4500
>150 and <250	0.4147	0.4447	0.4161	0.4252
>250	0.8482	0.8681	0.8153	0.8439

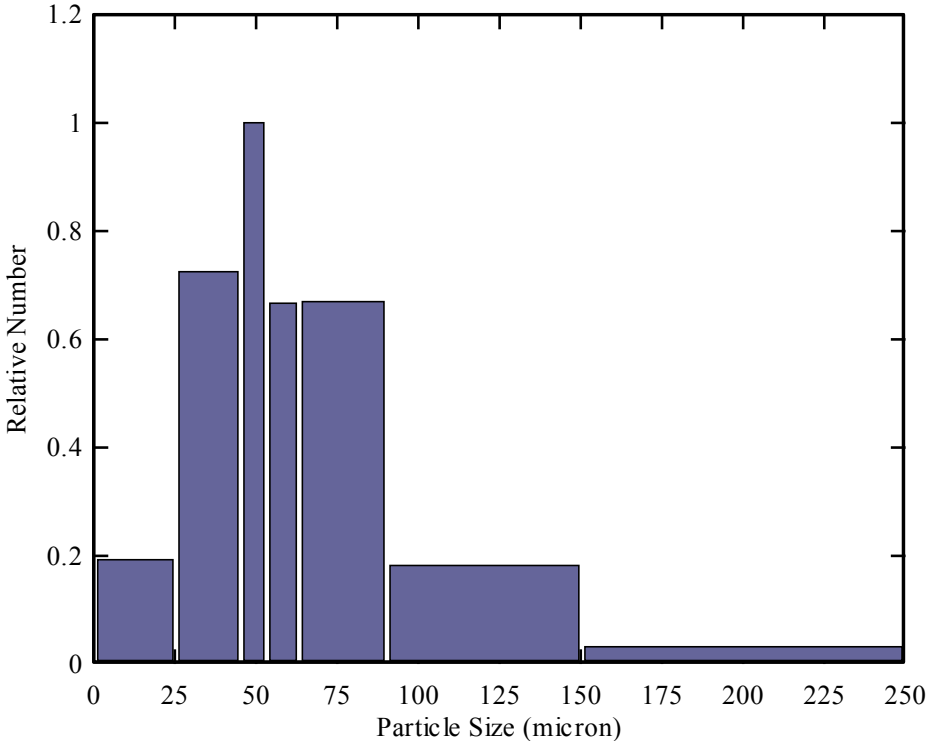

Figure 3-9. Particle Size Distribution of Received Uranium Oxide Powder

Characterization of the Silicon Carbide Whiskers

The silicon carbide (SiC) whiskers are commercially available from Alfa Aesar (Alfa) and Advanced Composite Materials (ACM). The whiskers from Alfa Aesar are 1.5 micron in diameter and about 18 micron in length (no detailed information available). The Whiskers from Advanced Composite Materials are 0.45-0.65 micron in diameter and 5-80 micron in length. Both of the whiskers are single crystal β-SiC. The received SiC whiskers were in the form of agglomerates. The scanning electron microscope (SEM) images of received SiC whiskers from Alfa Aesar are shown in Figure 3-10 and Figure 3-11. The X-ray diffraction pattern of SiC whiskers from Alfa Aesar is shown in Figure 3-12. The SEM images of the received SiC whiskers from Advanced Composite Materials are shown in Figure 3-13 and Figure 3-14. The X-ray diffraction pattern of SiC whiskers from Advanced Composite Materials are shown in Figure 3-15.

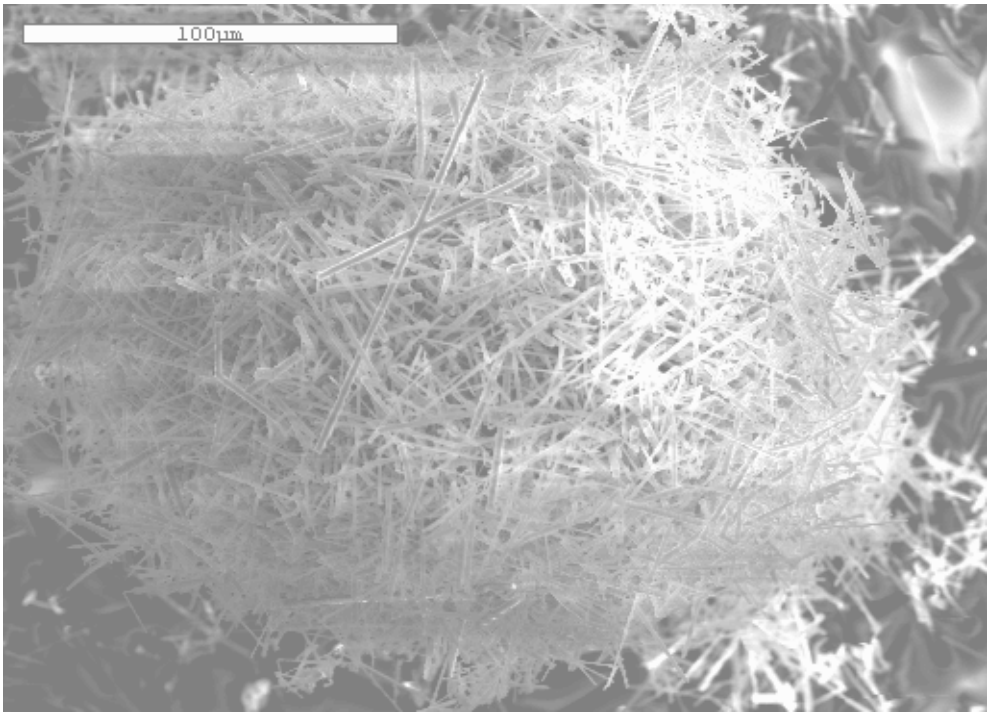

Figure 3-10. Scanning Electron Microscope Image of SiC Whiskers as Received from Alfa Aesar (500X)

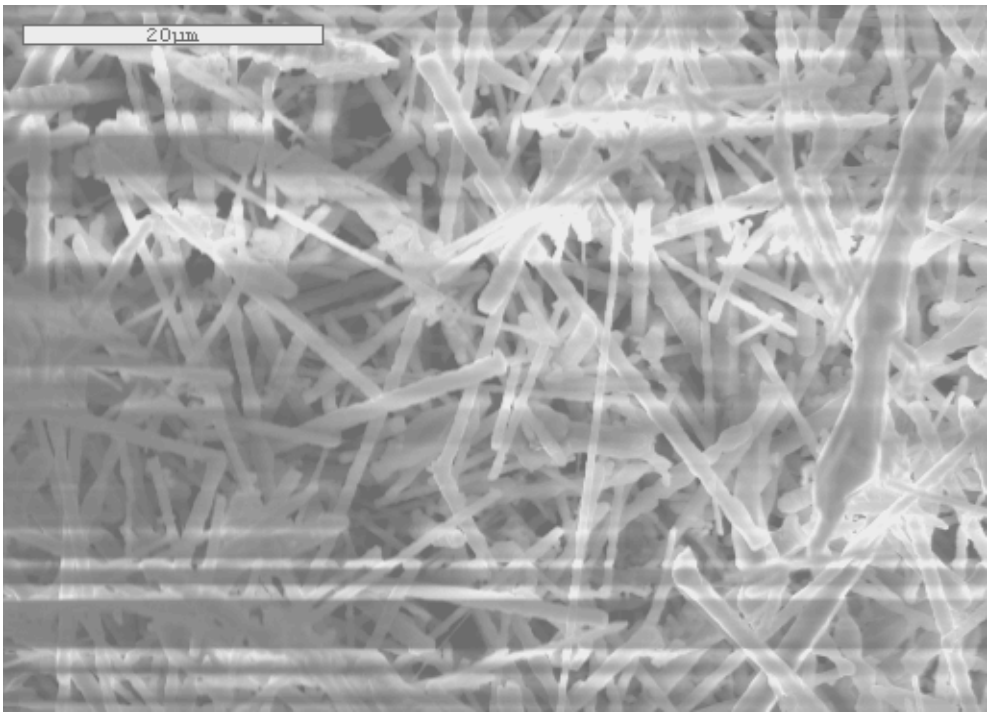

Figure 3-11. Scanning Electron Microscope Image of SiC Whiskers as Received from Alfa Aesar (2,000X)

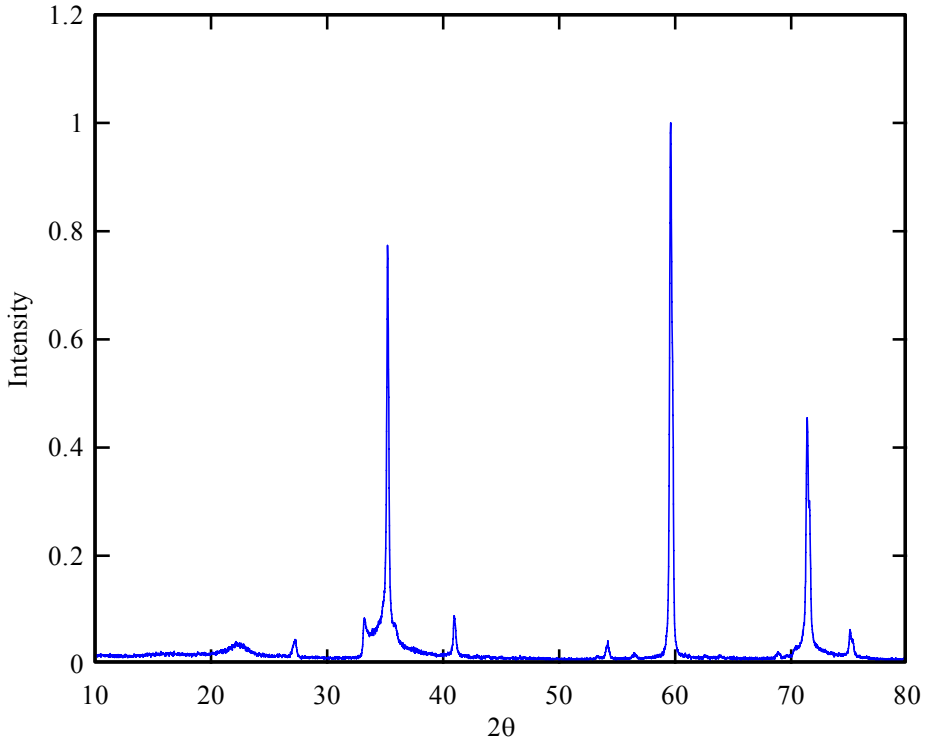

Figure 3-12. X-ray diffraction pattern of SiC whiskers from Alfa Aesar

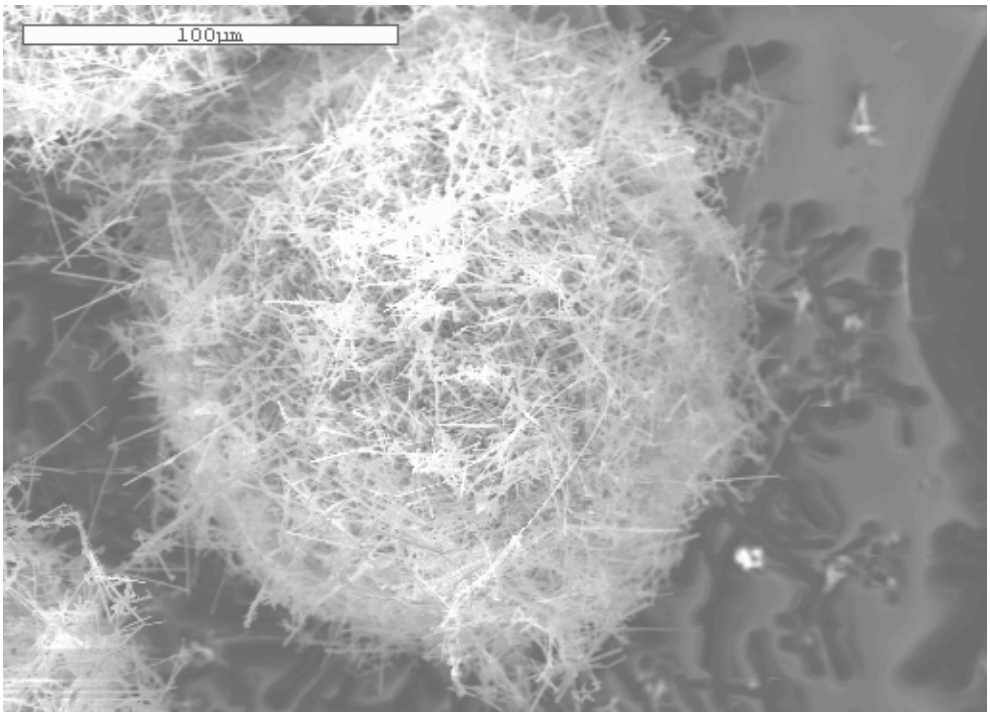

Figure 3-13. Scanning Electron Microscope Image of SiC Whiskers as Received from Advanced Composite Materials (500X)

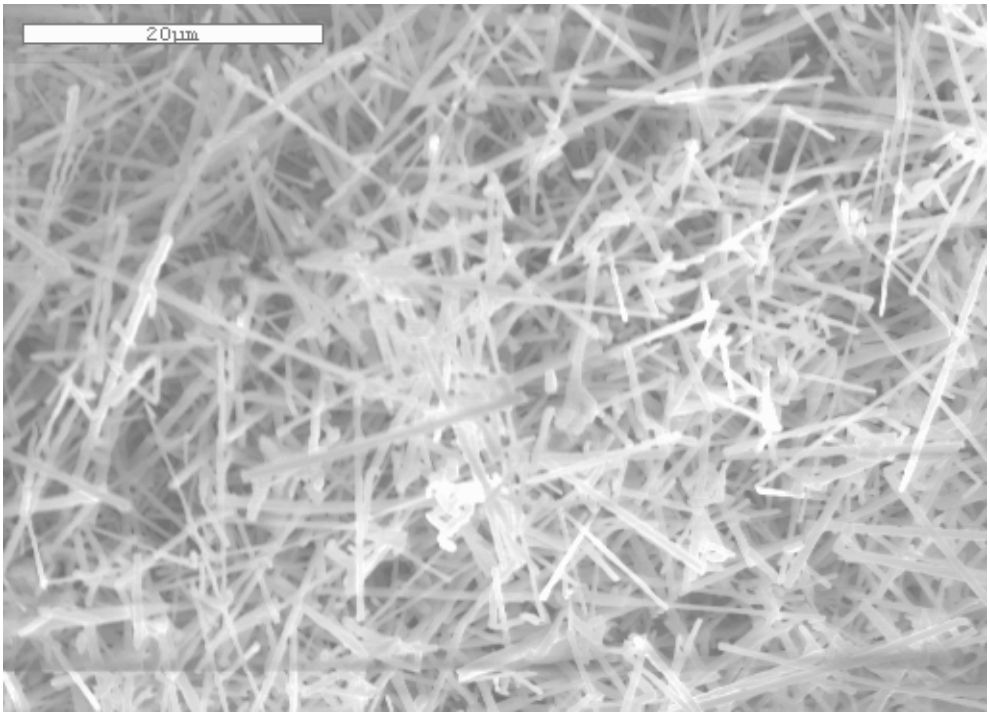

Figure 3-14. Scanning Electron Microscope Image of SiC Whiskers as Received from Advanced Composite Materials (2,000X)

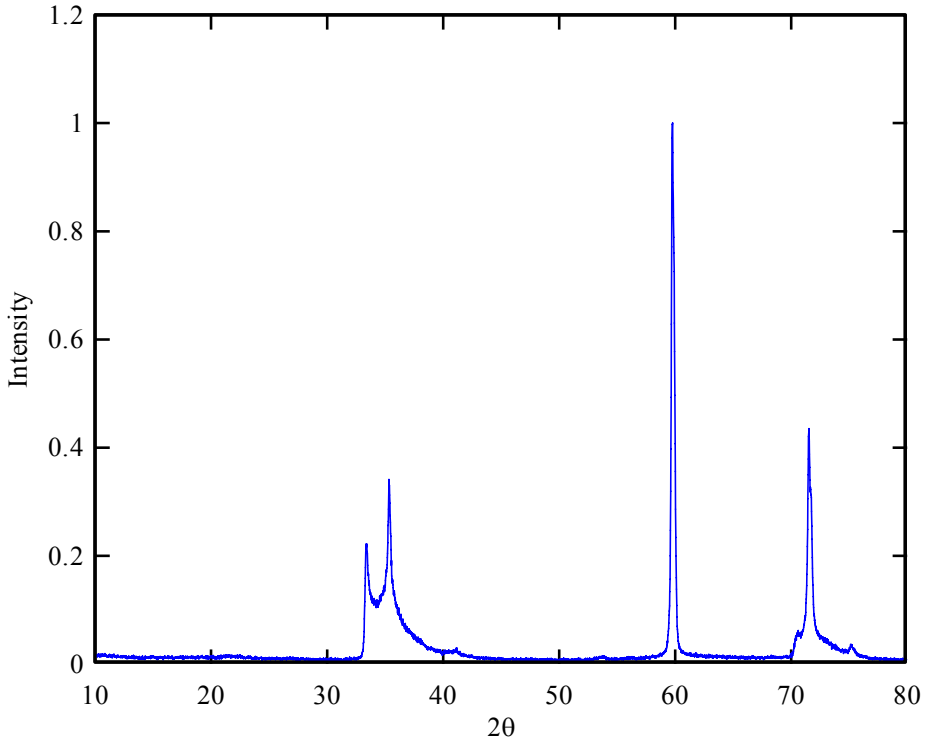

Figure 3-15. X-ray Diffraction Pattern of SiC Whiskers from Advanced Composite Materials

To separate the agglomeration, the received SiC whiskers were blended with distilled water in a blender for 3 minutes. A small amount of the mixture was dropped on the SEM sample holder, and the distilled water was left to evaporate, leaving only the separated SiC whiskers. Figure 3-16 and Figure 3-17 are the SEM images of dispersed SiC whisker from Alfa Aesar and Advanced Composite Materials, respectively. The SiC whiskers were successfully dispersed by the blending, based on the SEM images.

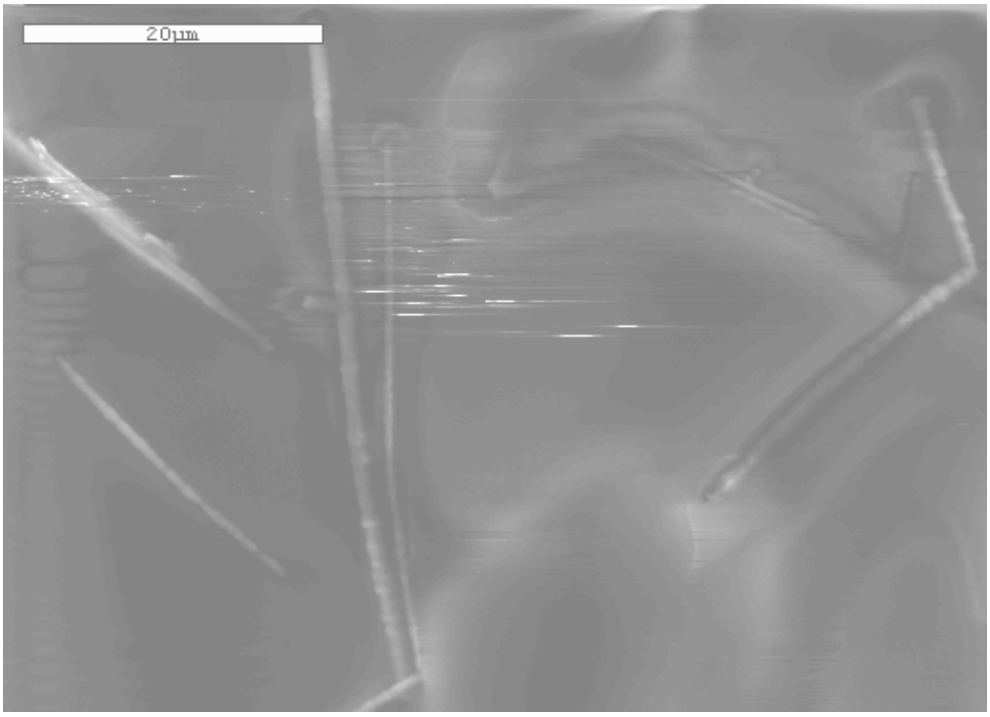

Figure 3-16. Scanning Electron Microscope Image of SiC Whiskers from Alfa Aesar after Dispersion (2,000X)

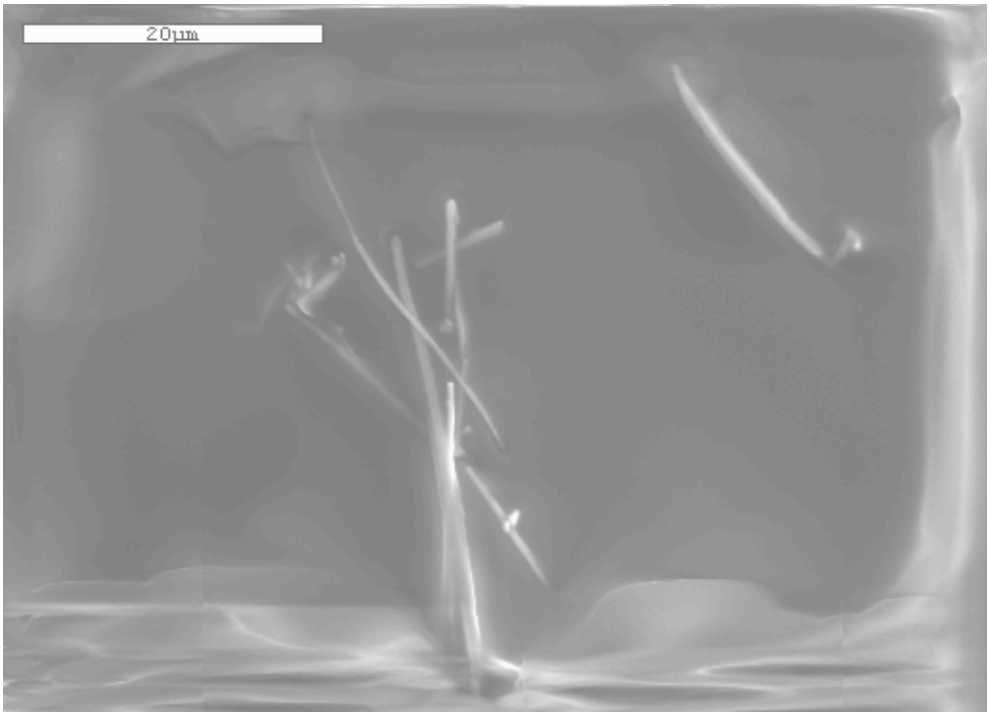

Figure 3-17. Scanning Electron Microscope Image of SiC Whiskers from Advanced Composite Materials after Dispersion (2,000X)

Reaction between Uranium Dioxide and Silicon Carbide

The reaction between uranium oxide (UO_2) and silicon carbide (SiC) was studied at different temperature. The received $UO_{2.10}$ powder was ball milled with the β-SiC powders (30 nm in particle size) from Alfa Aesar. The weight ratio of UO_2 to SiC is 1 to 1. Figure 3-18 shows the X-ray diffraction (XRD) pattern of the 30 nm β-SiC. The mixture powders were pressed at 200MPa, and then sintered at 1300 ^oC and 1650 ^oC. The pellets after sintering are shown in Figure 3-19 and Figure 3-21. There is no reaction between UO_2 and SiC at 1300 ^oC, as the XRD pattern shown in Figure 3-20. Reaction between UO_2 and SiC occurs at 1650 ^oC, and $USi_{1.88}$ (U_4Si_7) was formed, as shown in Figure 3-22.

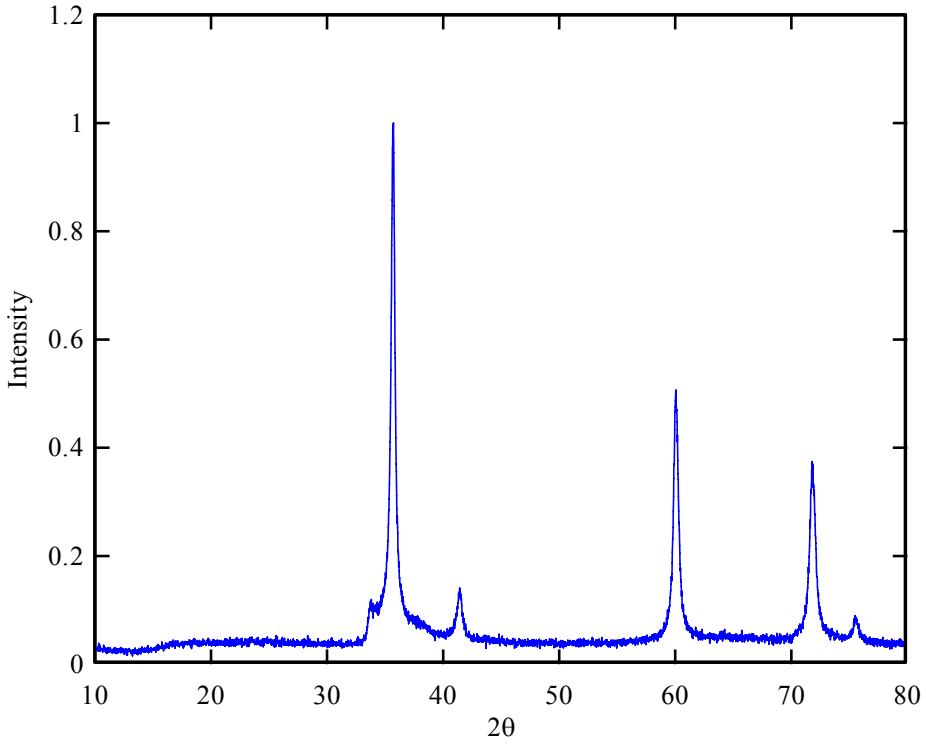

Figure 3-18. X-ray Diffraction Pattern of 30nm β-SiC from Alfa Aesar

Figure 3-19. UO_2-SiC pellet after sintering at 1300 ^oC

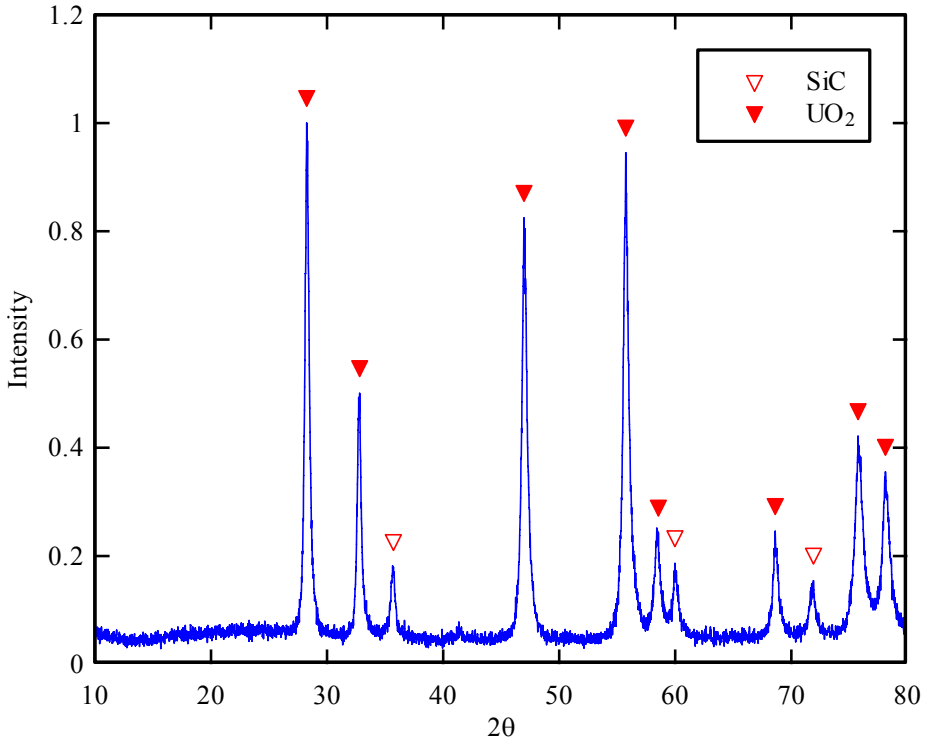

Figure 3-20. X-ray Diffraction Pattern of UO_2-SiC Pellet after Sintering at 1300 ^oC

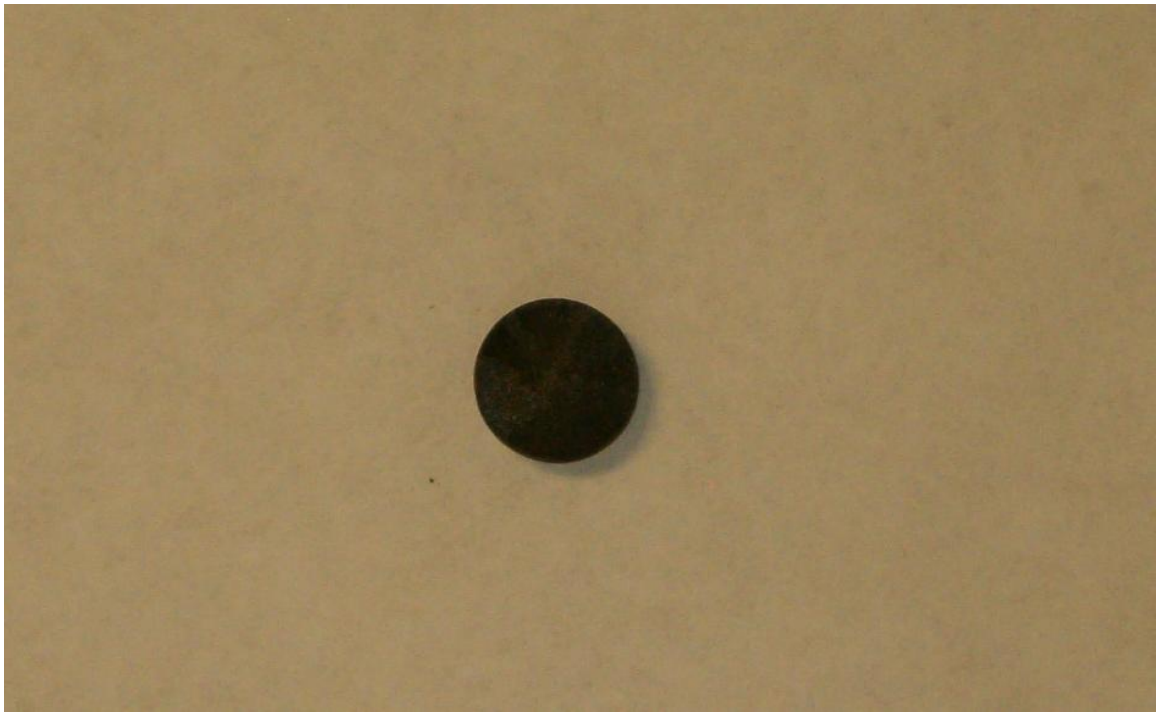

Figure 3-21. UO_2-SiC Pellet after Sintering at 1650 ^oC

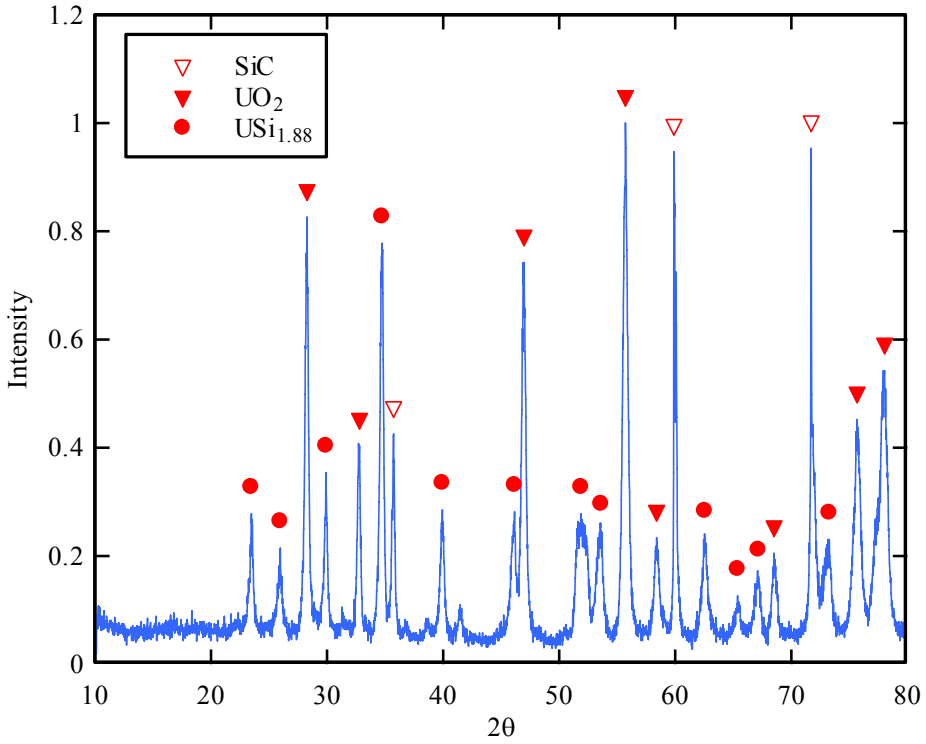

Figure 3-22. X-ray Diffraction Pattern of UO_2-SiC Pellet after Sintering at 1650 ^oC

Low Temperature Sintering of Uranium Dioxide

The received $UO_{2.10}$ was oxidized in air at 140 ^oC for 24 hours to increase the O/M ratio to $UO_{2.27}$. The $UO_{2.27}$ powder was then compacted in a 13mm die at 200 MPa pressure. The green pellet was sintered at 1200 ^oC for 1 hour in a nitrogen atmosphere, followed by the reduction in Ar+5% H_2 at 1200 ^oC for 3 hours. The top view of the sintered pellet is shown in Figure 3-23. The density of the pellet measured by Archimedes method was 94.56%TD.

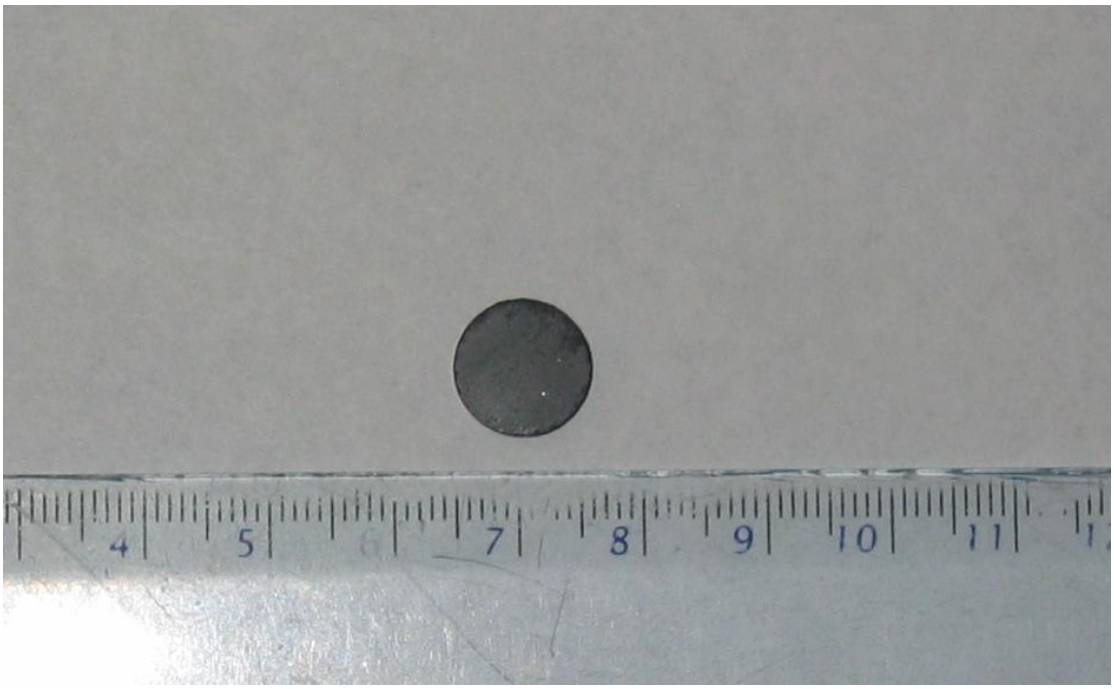

Figure 3-23. Pellet Sintered by Two Stages Low Temperature Sintering Method.

Silicon Carbide Whisker-Uranium Dioxide Composite

Received silicon carbide whiskers were first blended in distilled water for 3 minutes to separate the agglomeration. The separated SiC whiskers were then mixed with $UO_{2.27}$ particles in an ultrasonic mixer for 10 minutes. After the water was removed, the mixed powder was grounded by mortar and pestle. The mixed powder was then cold pressed in an alumina (Al_2O_3) die at 300MPa. The alumina die was made by an alumina tube and two alumina rods, which are shown in Figure 3-24. After cold pressing, the mixed powder and alumina die were placed in a sample holder and was surrounded by a graphite tube at the position of the mixed powder, as shown in Figure 3-25. The geometry of the alumina die and graphite tube is shown in Figure 3-26. The mixed powder was then hot press sintered in a hot press sintering apparatus, which included a sintering chamber, a high voltage alternating current (AC) generator and a pyrometer, as shown in Figure 3-27. The high voltage AC generator was connected to a copper coil inside

the sintering chamber. An alternating electromagnetic field was generated inside the coil when an AC current flowed through it. The changing electromagnetic field induced currents in the electrical conductor as it was placed inside the coil. The induced currents (Eddy current) generated heat inside the conductor due to the resistance. The alumina die and graphite tube was placed inside the coil. Eddy currents were induced inside the graphite tube, which is an electrical conductive material. Alumina and $UO_{2.27}$ are poor electrical conductors, so no Eddy currents were generated inside them. The surface temperature of the graphite tube was measured by the pyrometer. Figure 3-28 shows the heated graphite observed through the pyrometer. The pyrometer communicated with the high voltage AC generator to keep the surface temperature of the graphite tube constant as desired.

The surface temperature of the graphite tube is kept constantly at 1200 ^{o}C. The steady state temperatures of the alumina tube and mixed powder were calculated based upon Equation 3-1 and Equation 3-5. For the graphite tube,

$$\frac{1}{r}\frac{d}{dr}(r\frac{dT}{dr})+\frac{q'''}{k_g}=0 \qquad \text{Equation 3-1}$$

Where q''' is the rate of heat production per unit volume, and K_g is the thermal conductivity of graphite.

The two boundary conditions of the graphite tubs are Equation 3-2 and Equation 3-3.

$$\frac{dT}{dr}=0 \text{ at } r = 0.5 \text{ inch} \qquad \text{Equation 3-2}$$

$$T\,(r = 1 \text{ inch}) = 1200\ ^{o}\text{C} \qquad \text{Equation 3-3}$$

The heat flux on the surface of the graphite tube can be calculated by Equation 3-4.

$$q'' = \varepsilon\sigma T^4 \qquad \text{Equation 3-4}$$

Where ε is the emissivity, which is 0.95 for graphite, σ is the Stefan-Boltzmann constant, which equals to 5.67×10^{-8} W/m^2·K^4. The calculated graphite temperature at r = 0.5 inch is 1201.4 ^{o}C. For the alumina tube,

$$\frac{1}{r}\frac{d}{dr}\left(r\frac{dT}{dr}\right) = 0 \qquad \text{Equation 3-5}$$

The two boundary conditions of the graphite tubs are Equation 3-6 and Equation 3-7.

$$\frac{dT}{dr} = 0 \text{ at } r = 0.25 \text{ inch} \qquad \text{Equation 3-6}$$

$$T\,(r = 0.5 \text{ inch}) = 1201.4\ ^{o}\text{C} \qquad \text{Equation 3-7}$$

The calculated temperature of the alumina tube $T(r)$ is a constant, 1201.4 ^{o}C. The calculated temperature of the mixed powder is also a constant, 1201.4 ^{o}C using the same method as the alumina tube. The mixed powder was sintered at 1201.4 ^{o}C for 1 hour in an argon atmosphere. The pressure applied during the sintering process was about 10 MPa.

A total of eight pellets were made by the hot press sintering technique. The pellets, except for E3 and E4, were soaked in a hydrogen atmosphere for three hours to reduce O/U ratio. The composition of each pellet is shown in Table 3-3. One pellet (E13) was pure uranium oxide to serve as a reference. Silicon carbide whiskers from Alfa Asear were only used in pellet E11, and SiC whiskers form ACM were used in the rest of composites. The E3 and E4 pellets used uranium oxide particles less than 25 micron in size, while the rest used particles between 25 micron and 45 micron in size. The densities of the sintered pellets are in the range of 94.69 to 99.76% TD. The pictures of the pellets are shown in Figure 3-29 to Figure 3-36. The pellets were characterized by scanning electron microscope (SEM) and X-ray diffraction (XRD). The SEM images were shown in Figure 3-36 to Figure 3-52, and the XRD patterns were shown in Figure 3-53 to Figure 60.

Figure 3-24. Alumina Die for Hot Press Sintering.

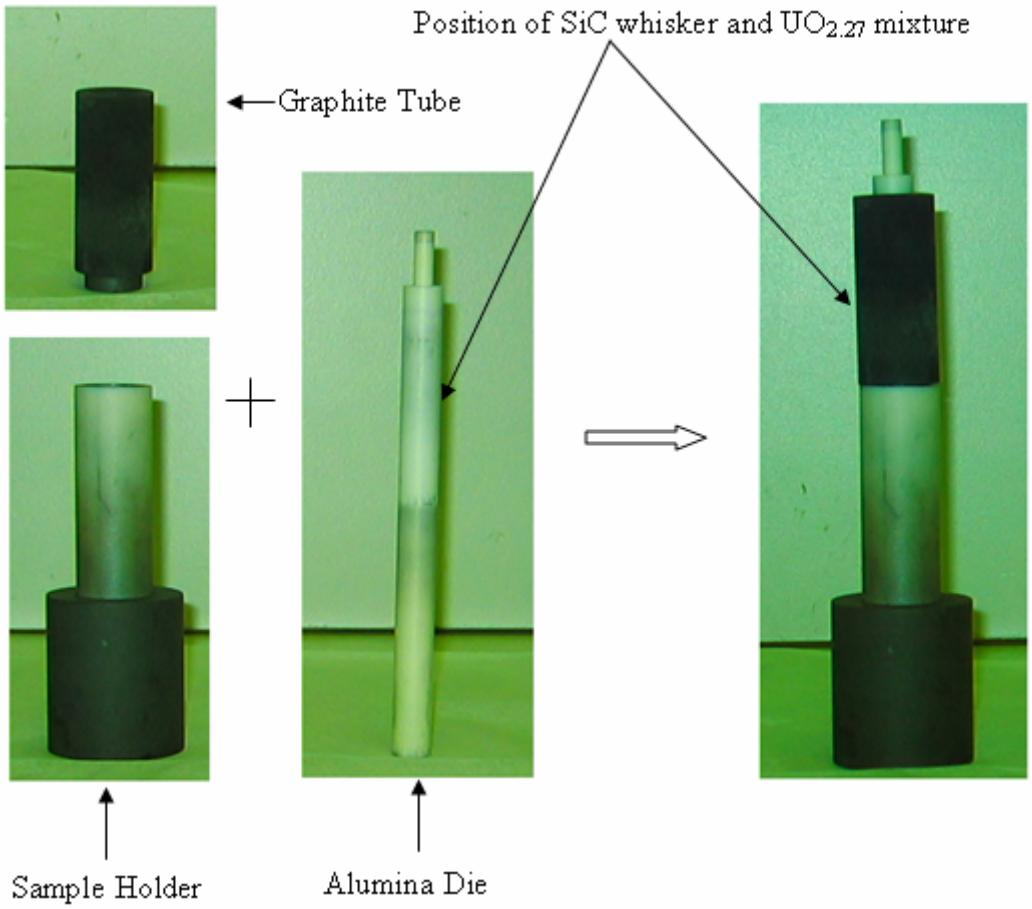

Figure 3-25. Alumina Die, Graphite Tube and Sample Holder.

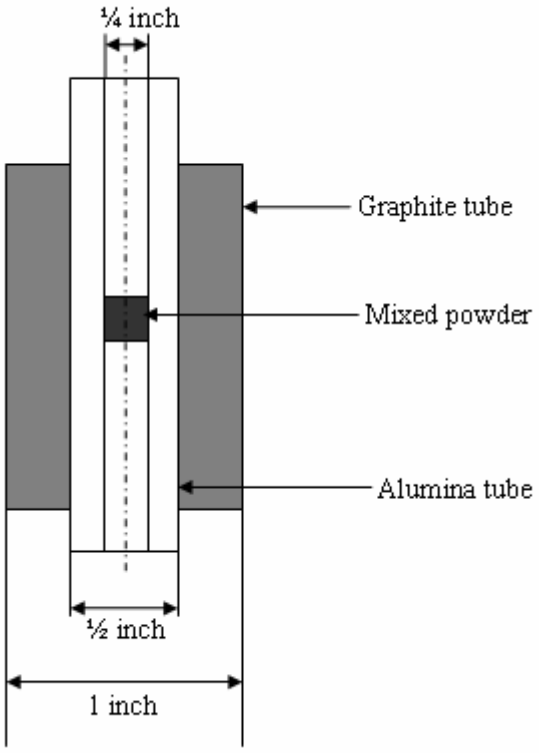

Figure 3-26. Geometry of the Alumina Die and Graphite Tube.

Figure 3-27. Hot Press Sintering Apparatus.

Figure 3-28. Heated Graphite Tube Observed Through the Pyrometer.

Table 3-3. The Silicon Carbide Whisker-Uranium Oxide Composites by Hot Press Sintering.

Experiment	UO_2 Size (μm)	SiC Type	Vol % of SiC	Vol % of UO_2	TD (g/cm^3)	Density (%)
E3	25	ACM	15	85	9.8	95.63
E4	25	ACM	30	70	8.64	95.81
E6	45	ACM	5	95	10.57	95.40
E7	45	ACM	10	90	10.19	94.69
E8	45	ACM	15	85	9.8	98.76
E14	45	ACM	30	70	8.64	97.79
E11	45	Alfa Aesar	15	85	9.8	99.76
E13	45	N/A	0	100	10.96	97.99

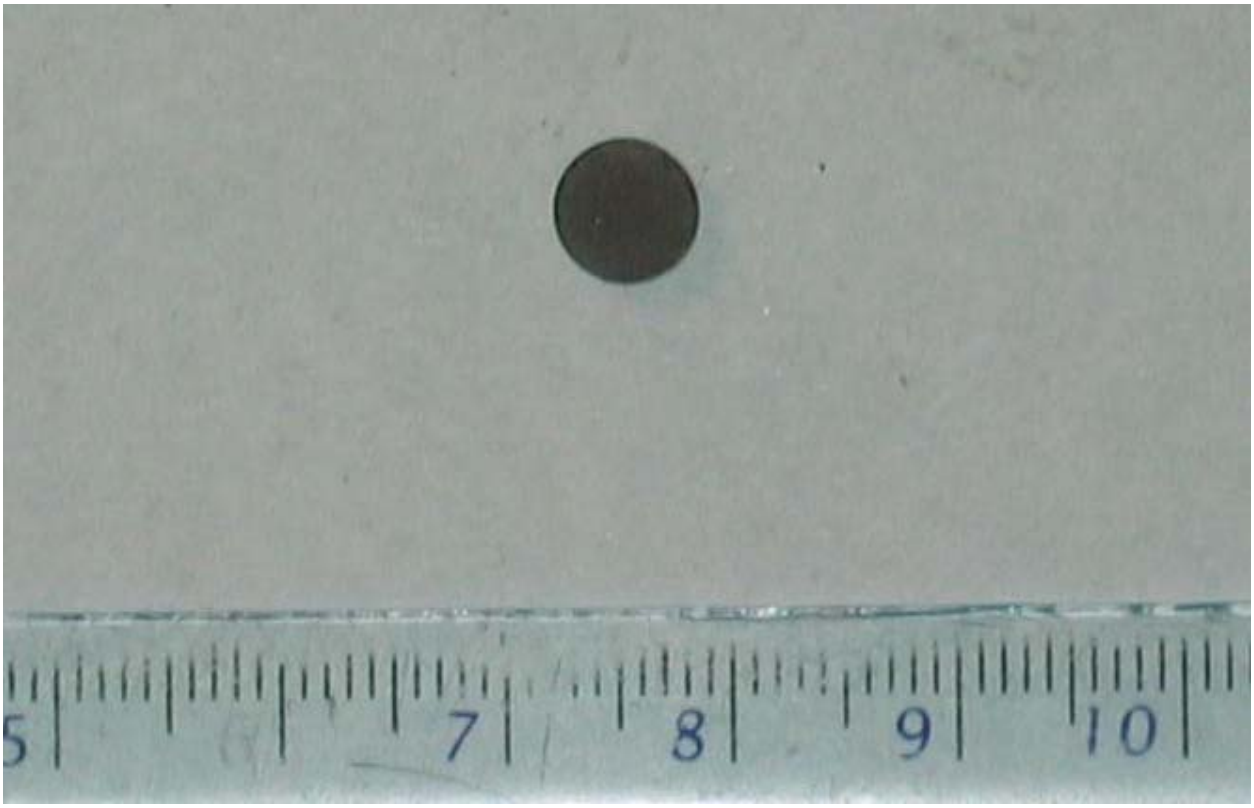

Figure 3-29. Picture of Pellet E3.

Figure 3-30. Picture of Pellet E4.

Figure 3-31. Picture of Pellet E6.

Figure 3-32. Picture of Pellet E7.

Figure 3-33. Picture of Pellet E8.

Figure 3-34. Picture of Pellet E14.

Figure 3-35. Picture of Pellet E11.

Figure 3-36. Picture of Pellet E13.

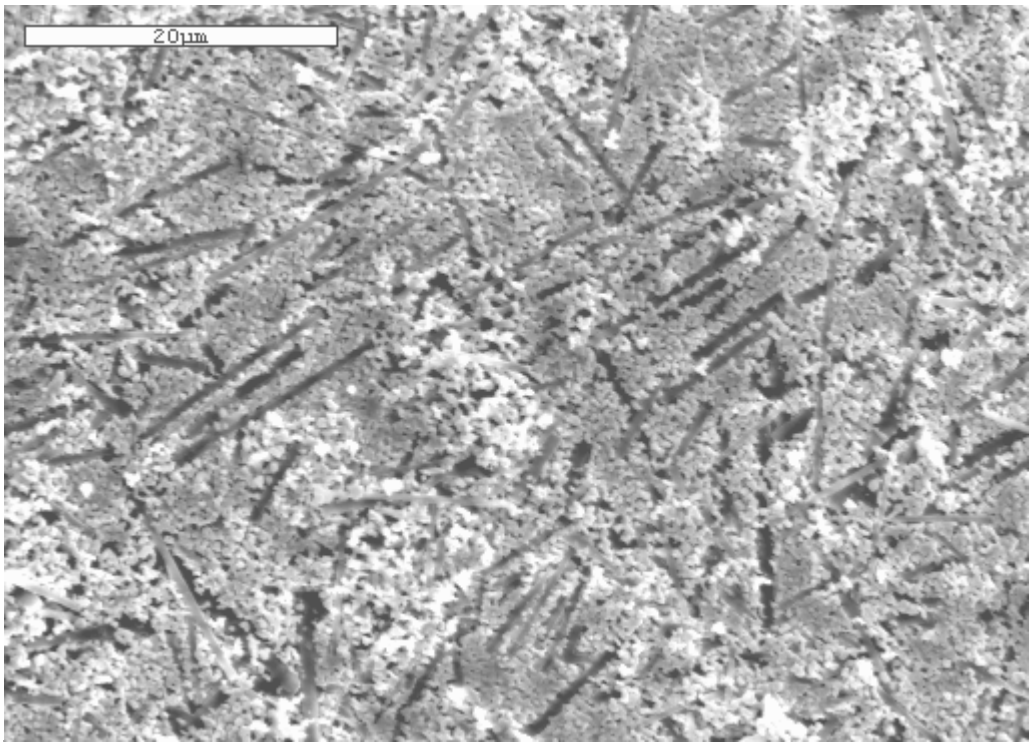

Figure 3-37. Scanning Electron Microscope Image of Pellet E3 (2,000X).

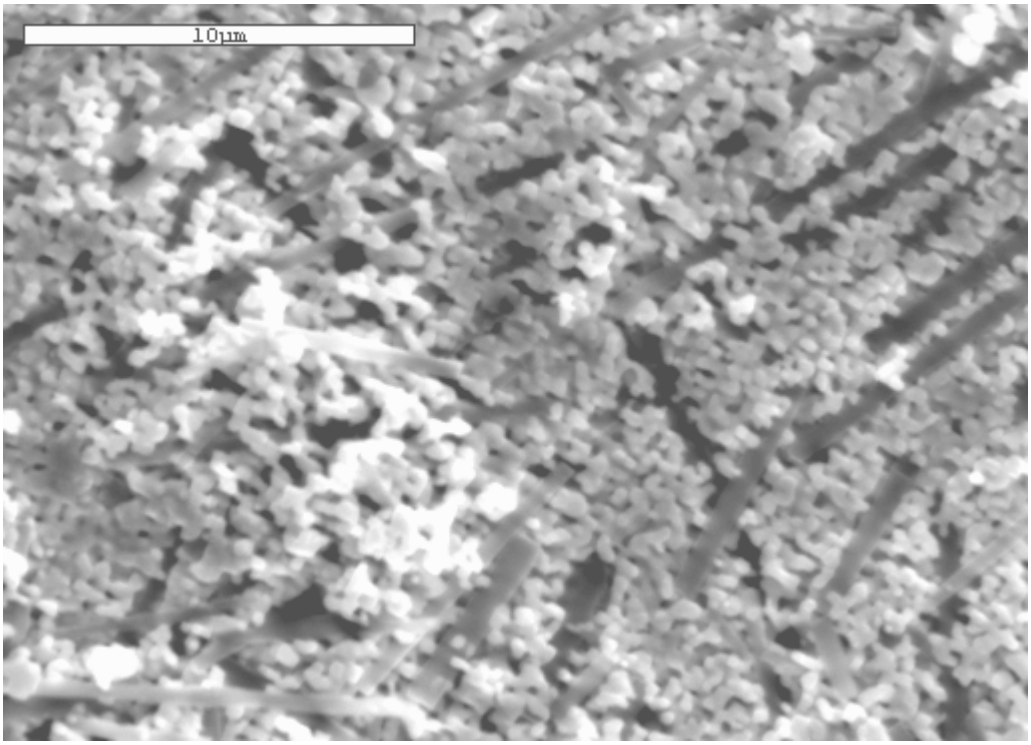

Figure 3-38. Scanning Electron Microscope Image of Pellet E3 (5,000X).

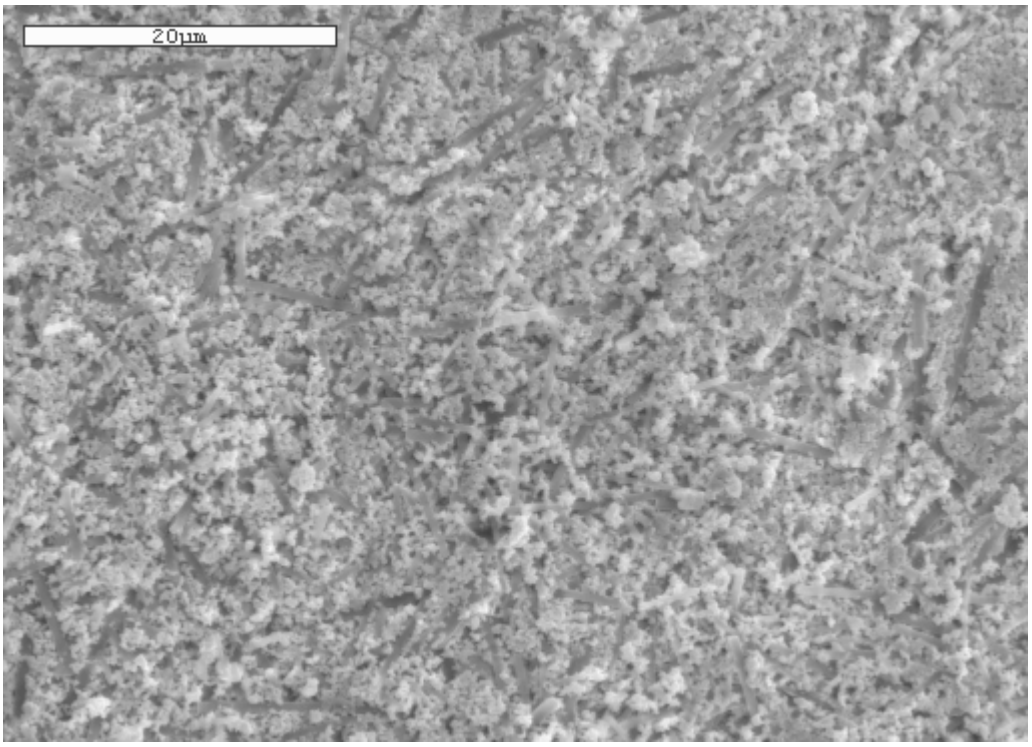

Figure 3-39. Scanning Electron Microscope Image of Pellet E4 (2,000X).

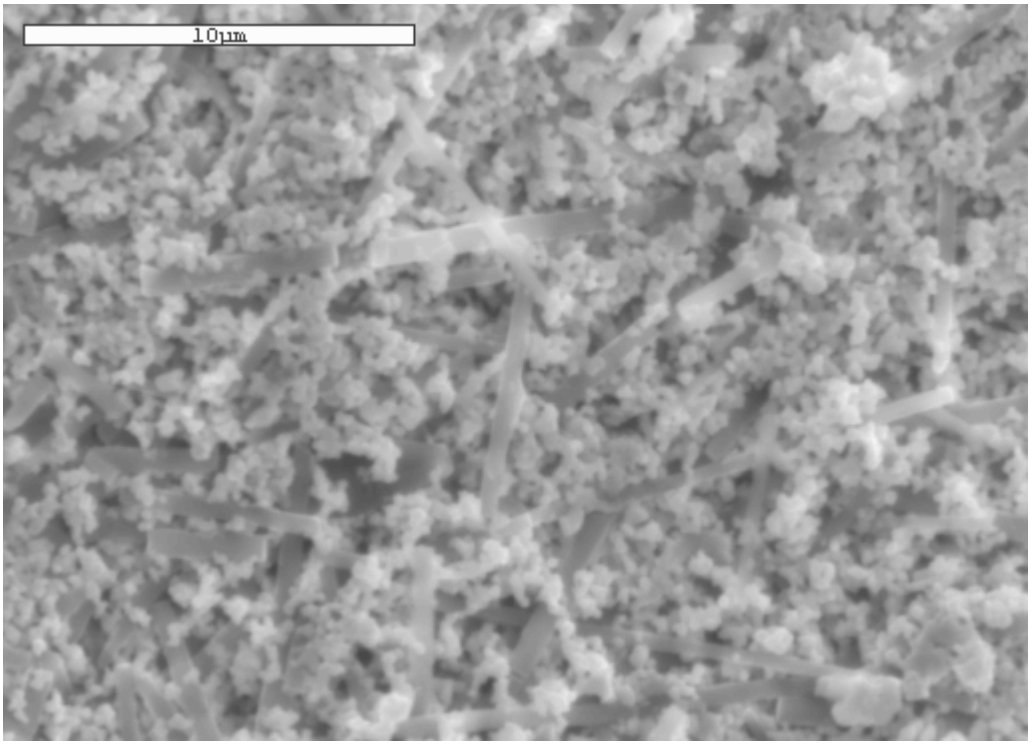

Figure 3-40. Scanning Electron Microscope Image of Pellet E4 (5,000X).

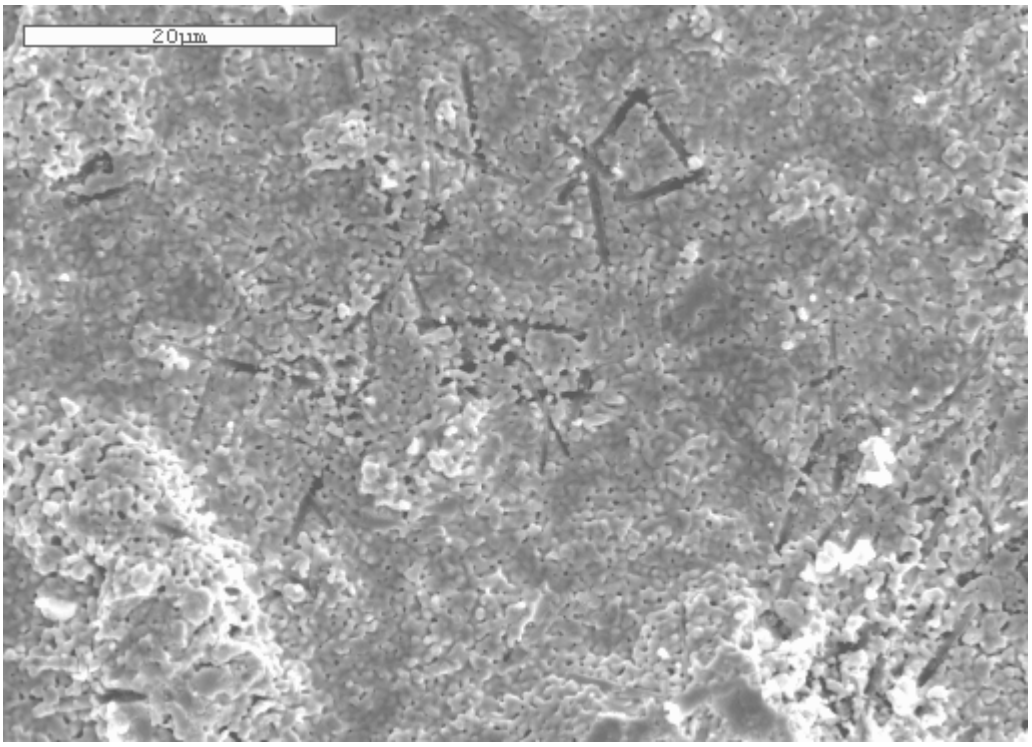

Figure 3-41. Scanning Electron Microscope Image of Pellet E6 (2,000X).

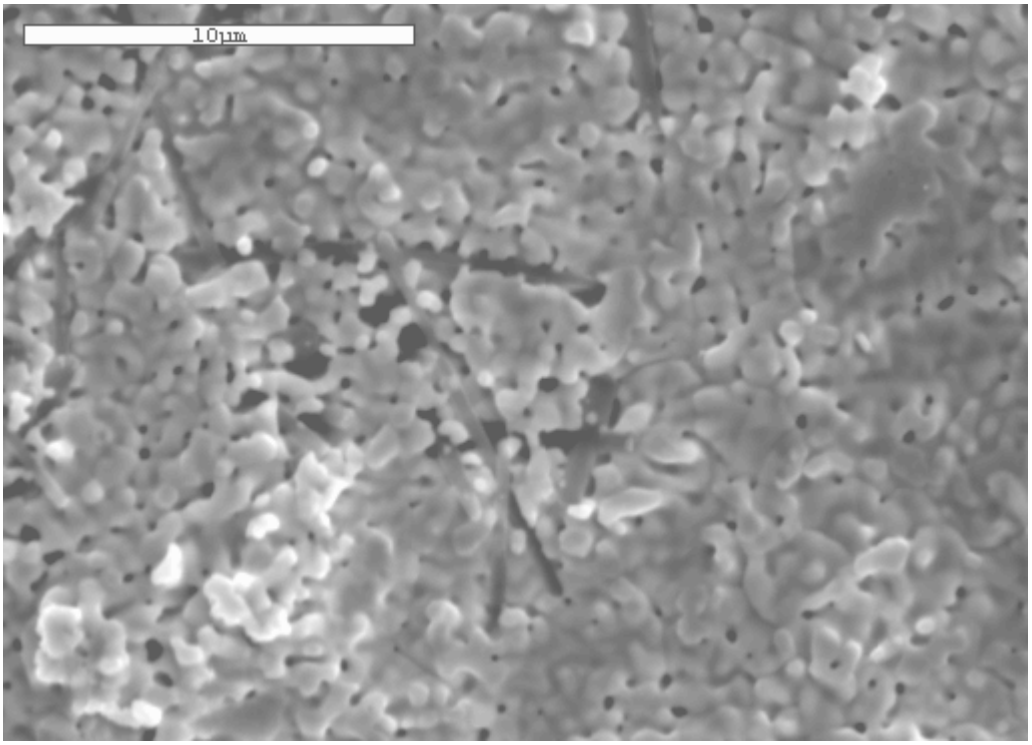

Figure 3-42. Scanning Electron Microscope Image of Pellet E6 (5,000X).

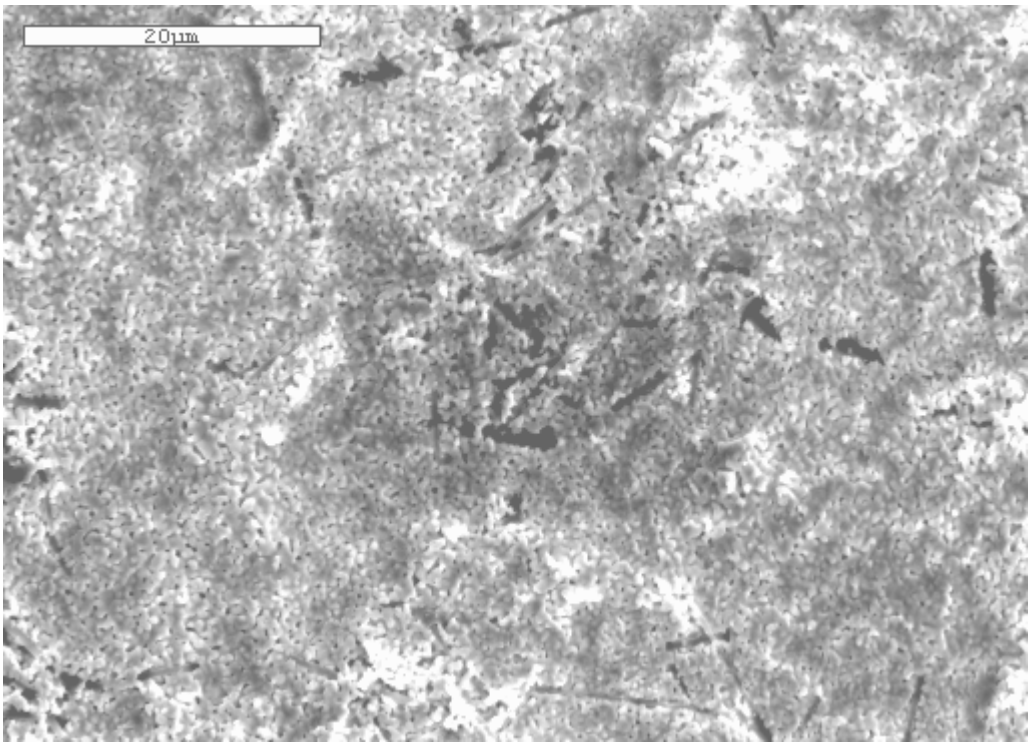

Figure 3-43. Scanning Electron Microscope Image of Pellet E7 (2,000X).

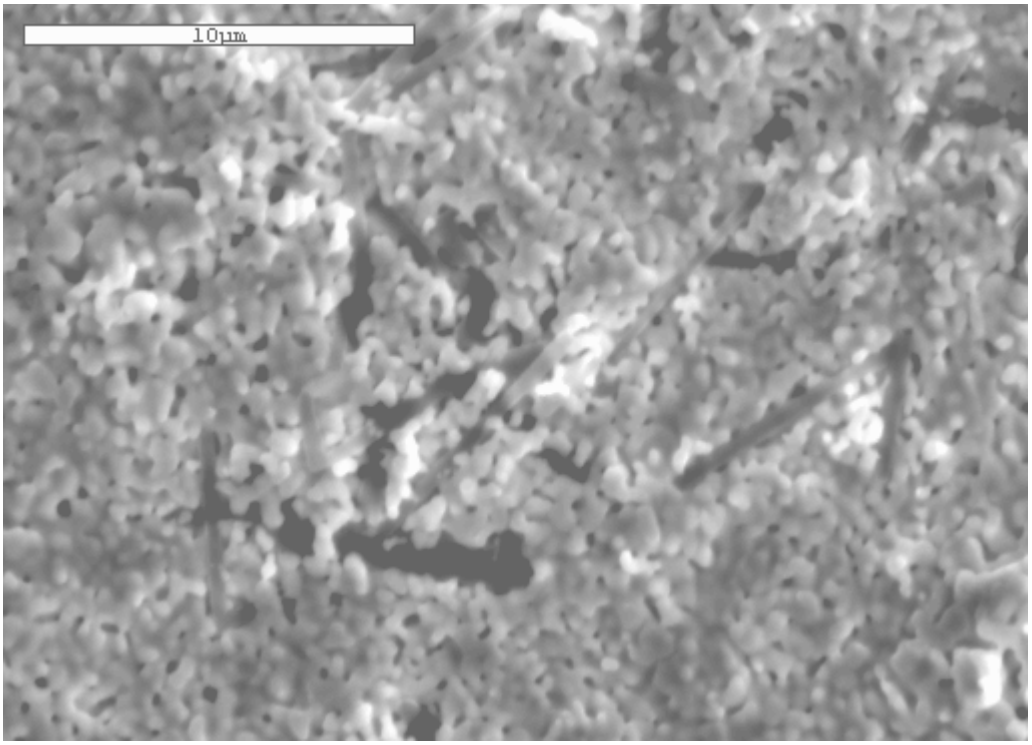

Figure 3-44. Scanning Electron Microscope Image of Pellet E7 (5,000X).

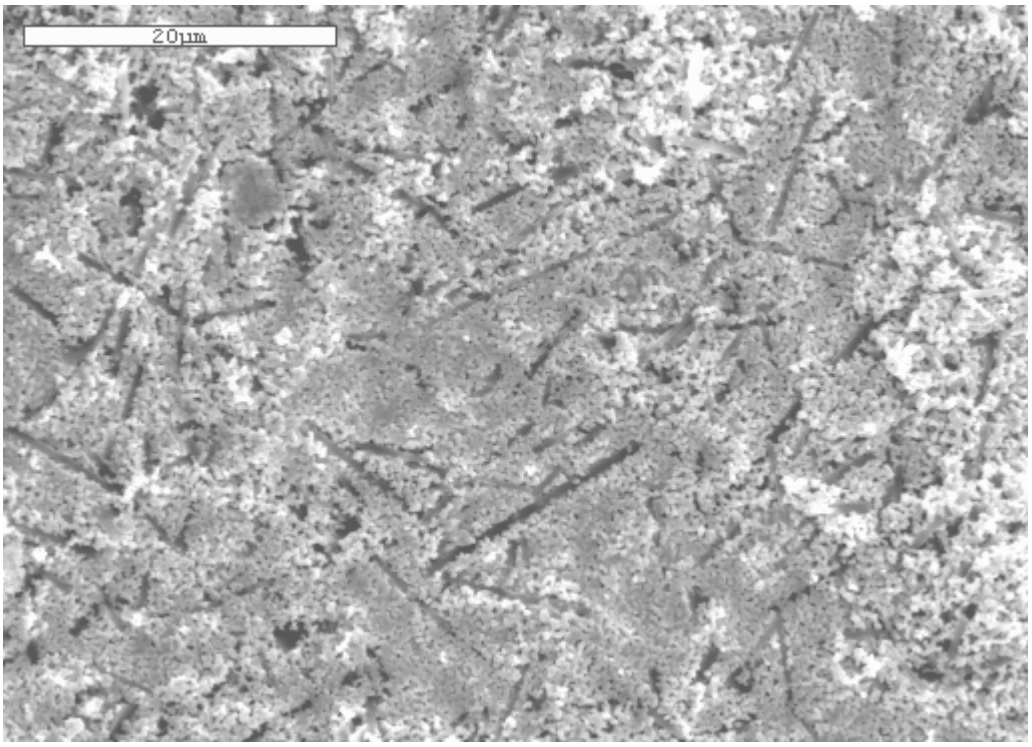

Figure 3-45. Scanning Electron Microscope Image of Pellet E8 (2,000X).

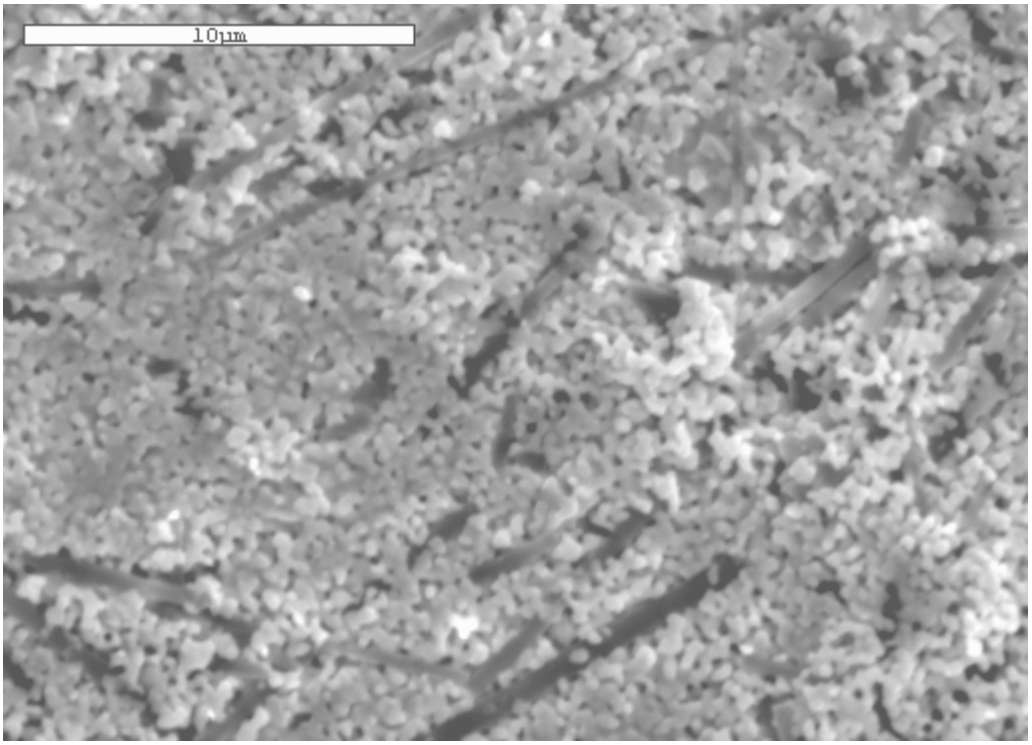

Figure 3-46. Scanning Electron Microscope Image of Pellet E8 (5,000X).

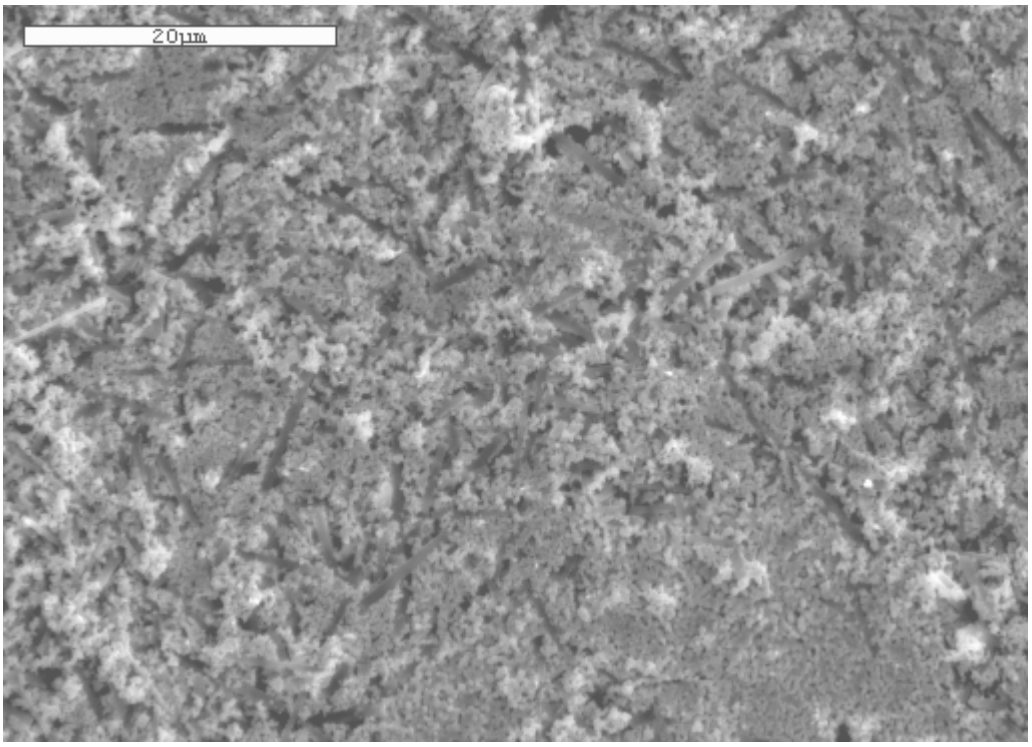

Figure 3-47. Scanning Electron Microscope Image of Pellet E14 (2,000X).

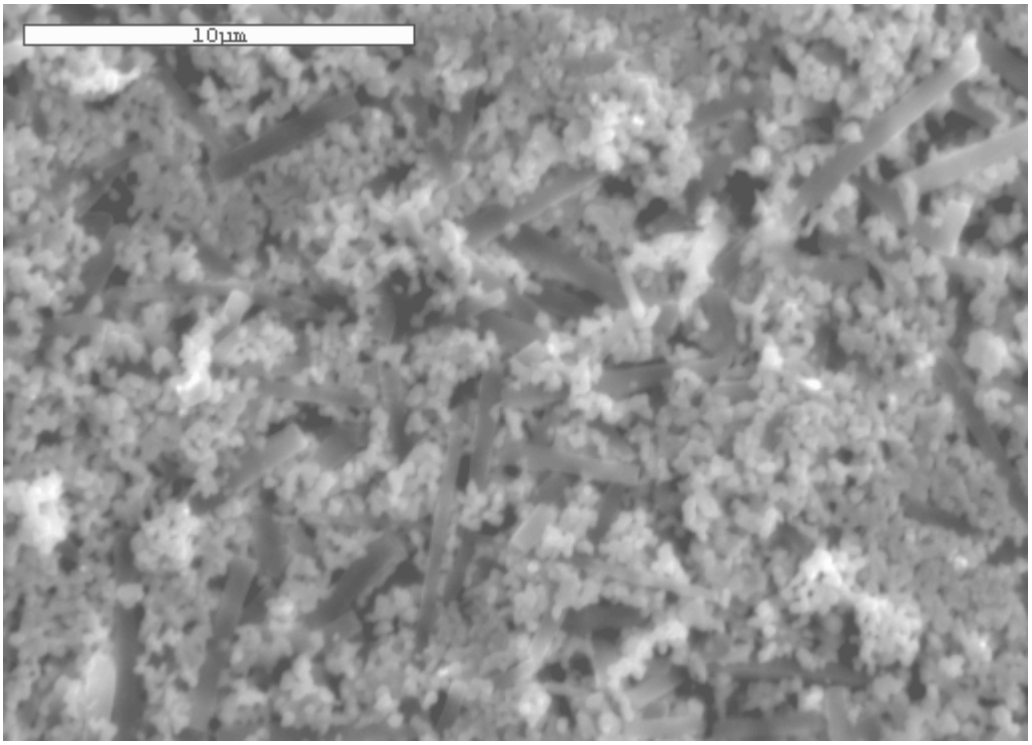

Figure 3-48. Scanning Electron Microscope Image of Pellet E14 (5,000X).

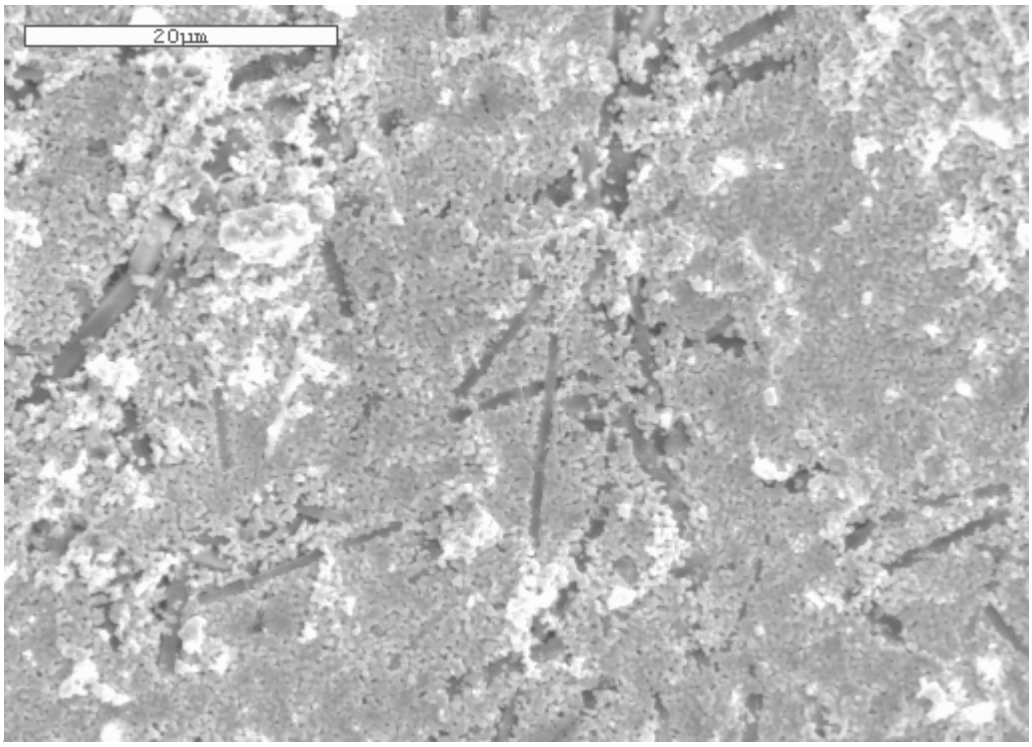

Figure 3-49. Scanning Electron Microscope Image of Pellet E11 (2,000X).

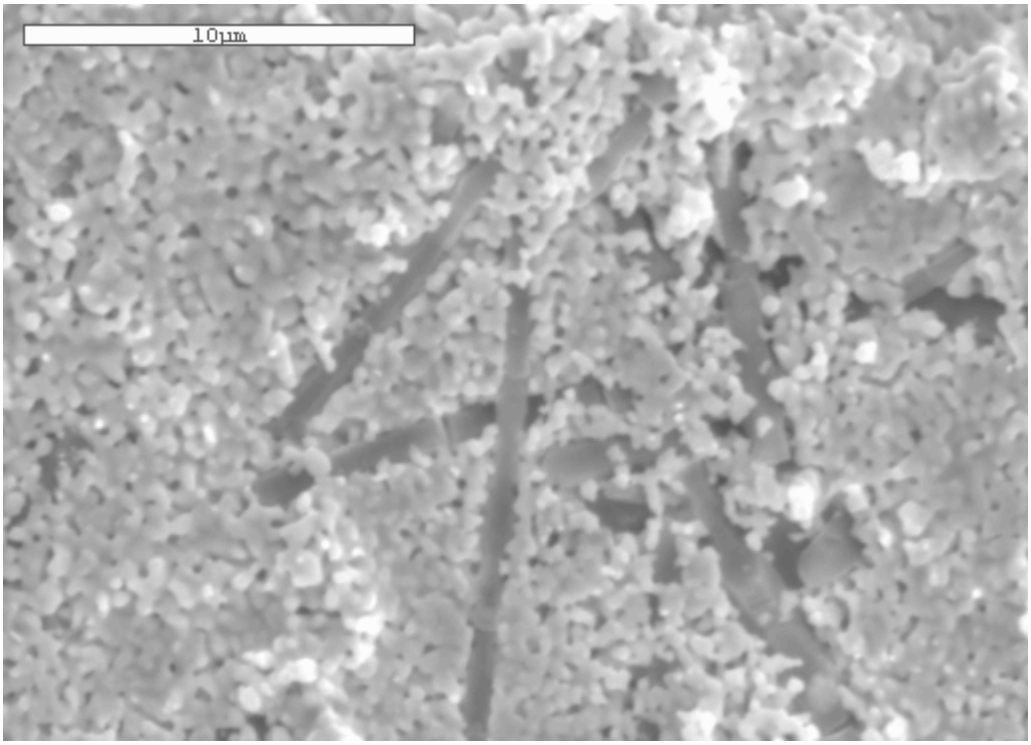

Figure 3-50. Scanning Electron Microscope Image of Pellet E11 (5,000X).

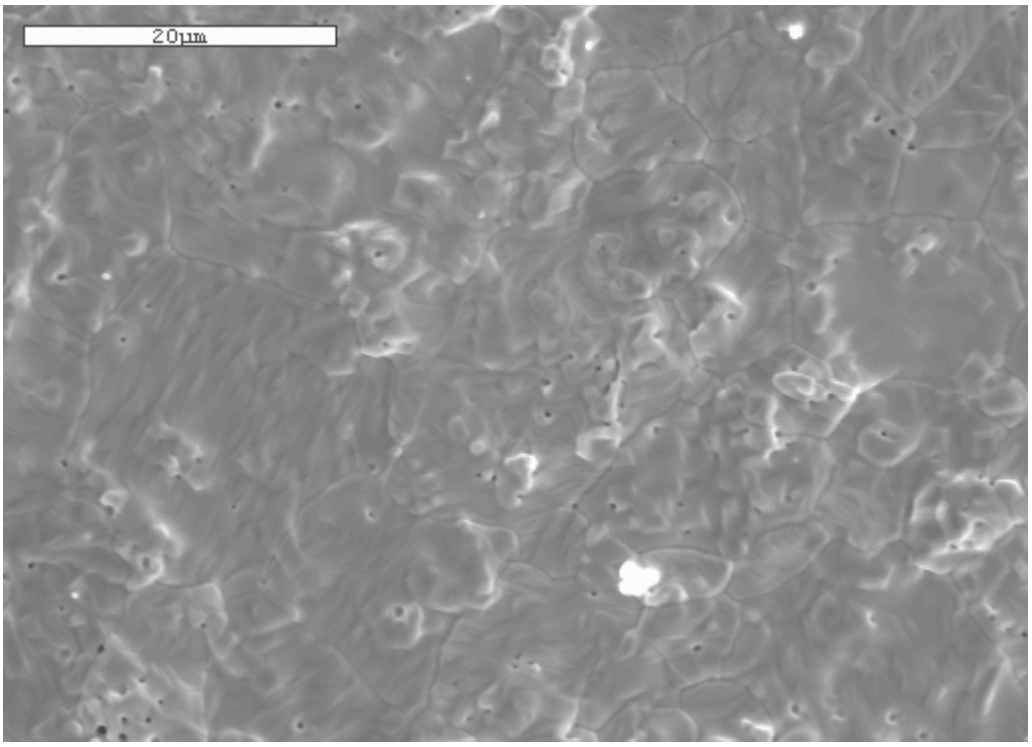

Figure 3-51. Scanning Electron Microscope Image of Pellet E13 (2,000X).

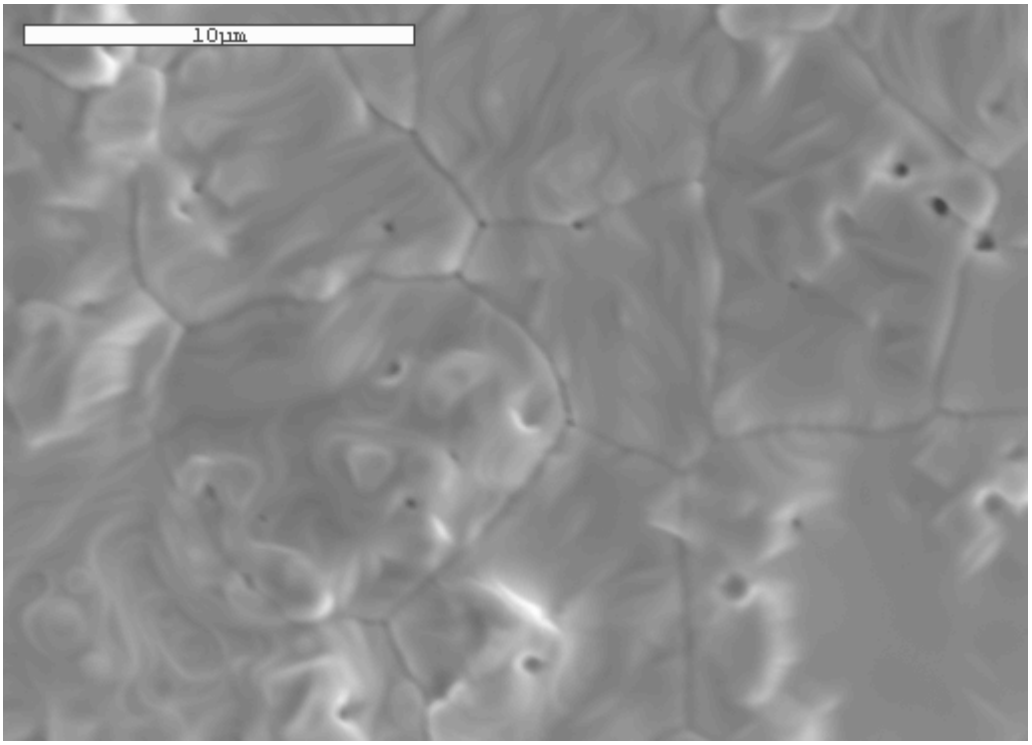

Figure 3-52. Scanning Electron Microscope Image of Pellet E13 (5,000X).

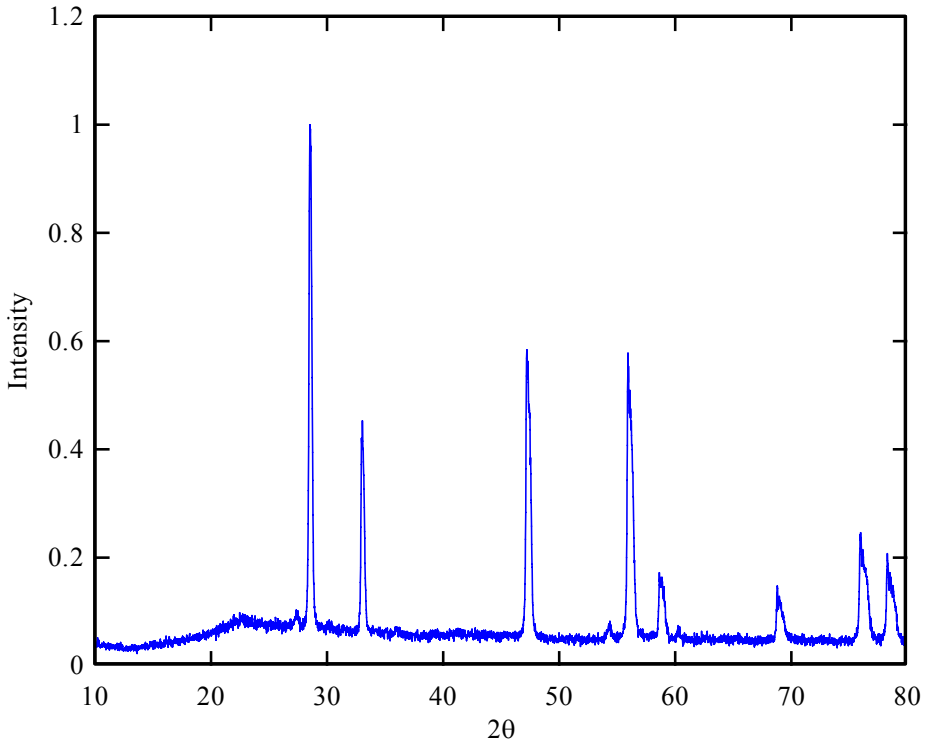

Figure 3-52. X-ray Diffraction Pattern of Pellet E3.

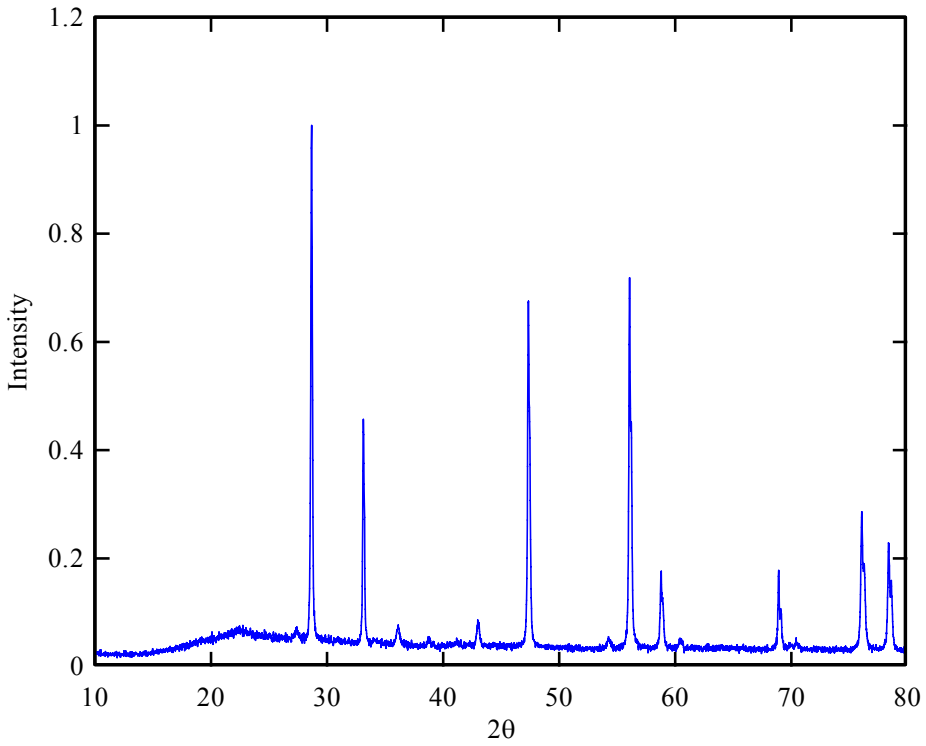

Figure 3-54. X-ray Diffraction Pattern of Pellet E4.

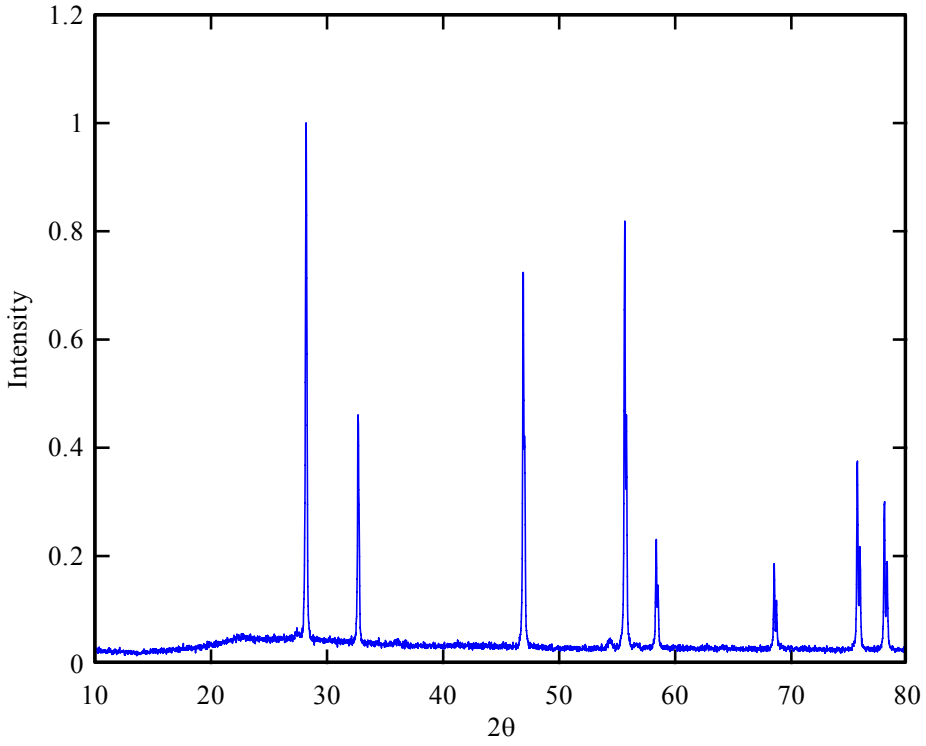

Figure 3-55. X-ray Diffraction Pattern of Pellet E6.

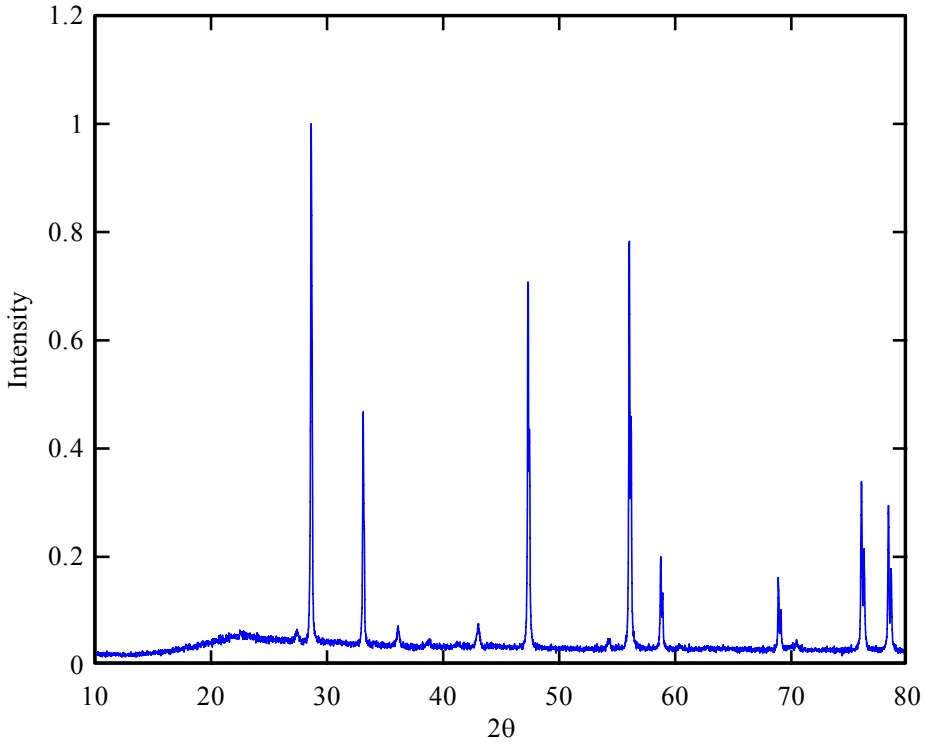

Figure 3-56. X-ray Diffraction Pattern of Pellet E7.

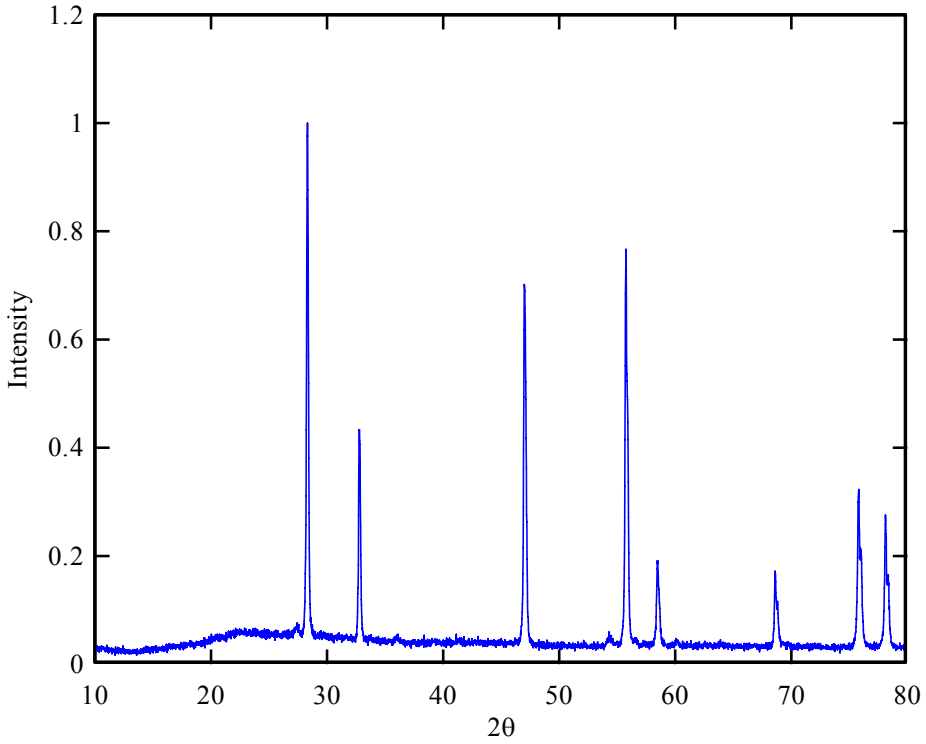

Figure 3-57. X-ray Diffraction Pattern of Pellet E8.

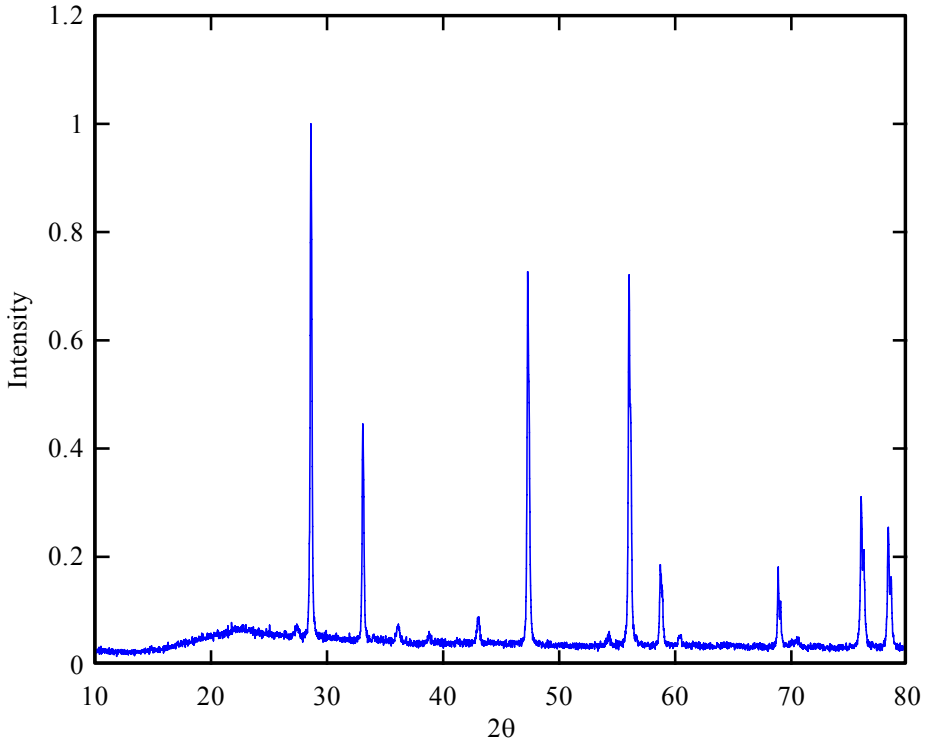

Figure 3-58. X-ray Diffraction Pattern of Pellet E14.

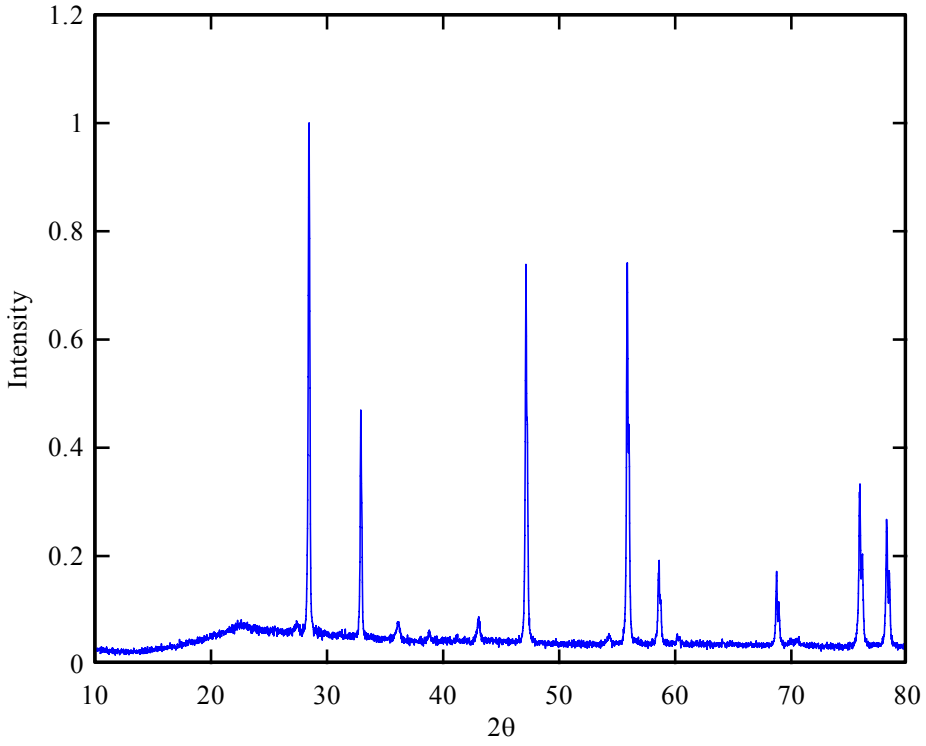

Figure 3-59. X-ray Diffraction Pattern of Pellet E11.

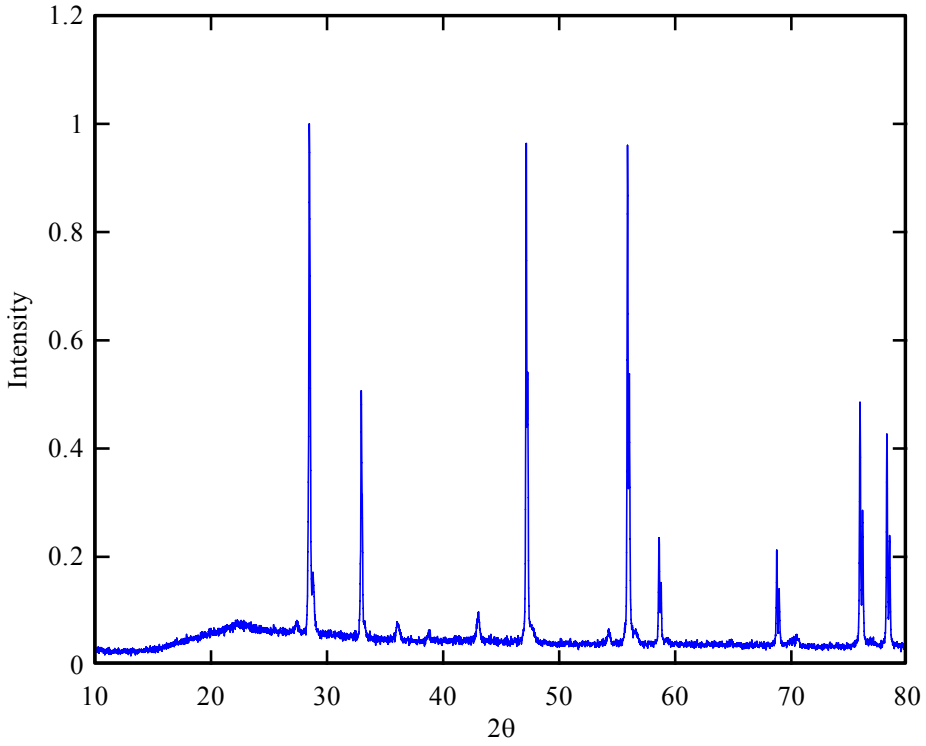

Figure 3-60. X-ray Diffraction Pattern of Pellet E13.

Silicon Carbide Coating by Polymer Precursor

Crystalline silicon carbide can be produced by decomposition of a commercially available polymeric precursor, allylhydridopolycarbosilane (AHPCS). The AHPCS, also called "SMP-10" by the manufacturer (Starfires Systems Inc.), is liquid with bright orange color, as shown in Figure 3-61. Uranium oxide ($UO_{2.27}$) powder was mixed with 10 weight % AHPCS in hexane (C_6H_{14}). After the hexane evaporated, the mixed powder was first cold pressed in an alumina die (¼ inch in diameter) at 300 MPa, and then both the pellet and the alumina die were sintered in argon atmosphere in a Lindberg/Blue Mini-Mite furnace (Figure 3-62). The heating rate from room temperature to 250 ^{o}C was 2 ^{o}C/min; the heating rate from 250 ^{o}C to 650 ^{o}C was 1 ^{o}C/min; the heating rate from 650 ^{o}C to 850 ^{o}C was 3 ^{o}C/min. The temperature was hold at 850 ^{o}C for 1 hour, and then decrease to room temperature at a rate of 3 ^{o}C/min. During the sintering process, about 70 MPa pressure was applied on the pellet. The pressure was provided by two springs located at the end of the furnace tube, which was sealed by stainless steel end caps.

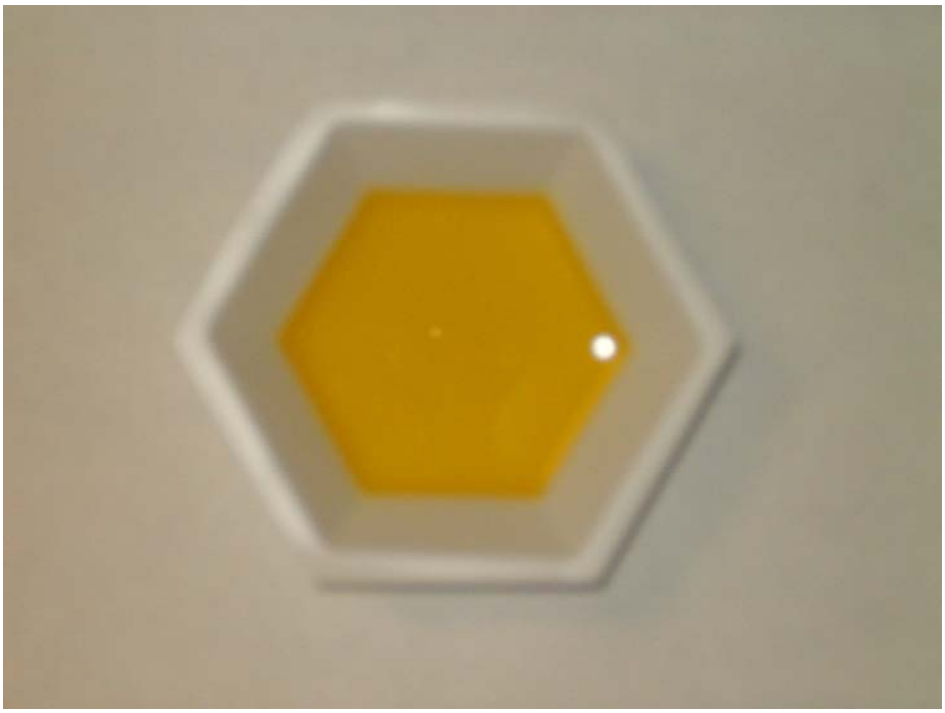

Figure 3-61. Allylhydridopolycarbosilane (AHPCS), the Polymer Precursor of Silicon Carbide.

Figure 3-62. Lindberg/Blue Mini-Mite Furnace.

After sintering, the pellet was broken when it was taken out of the alumina die. The probable reason for the lack of success is that the polymer precursor was oxidized by the $UO_{2.27}$ powder. The polymer precursor was oxidized by the extra oxygen in the uranium oxide powder before it can be converted to silicon carbide.

Silicon Carbide Coating by Chemical Vapor Deposition

The chemical vapor deposition (CVD) process was used to deposit β-SiC coating on the UO_2 particles. A buffer carbon layer was deposited on the UO_2 particles by decomposition of propane (C_3H_8) prior to SiC deposition. The CVD process was carried out at 1300 ^oC using a Lindberg Blue high temperature tube furnace as shown in Figure 3-63. Argon and 5% H_2 gas was used as carrier gas at a constant flow rate of 140 sccm (cm^3/min). Propane flowed through the furnace at the flow rate of 5 sccm (cm3/min) at the temperature of 1300 ^oC for 5 minutes.

The precursor, TMS, flowed through the furnace at the flow rate of 5 sccm at the temperature of 1300 ^{o}C for 30 minutes. Figure 3-64 shows the powder after the CVD process.

Fourier Transform Infrared Spectroscopy (FTIR) and X-ray Diffraction (XRD) were used to characterize the SiC coating after the CVD processing. FTIR was used to obtain information about the chemical bonding in the material. XRD was used to identify the crystalline structure. The FTIR result is shown in Figure 3-65. The UO_2 powder after CVD process has a peak at the same position as SiC powder, which indicates the formation of Si-C bond; however, there is no SiC peak in the XRD pattern, as shown in Figure 3-66. The probable reason is that the amorphous SiC was formed instead of crystalline silicon carbide.

Figure 3-63. Lindberg High Temperature Furnace.


Figure 3-64. Uranium Dioxide Powder after CVD of SiC

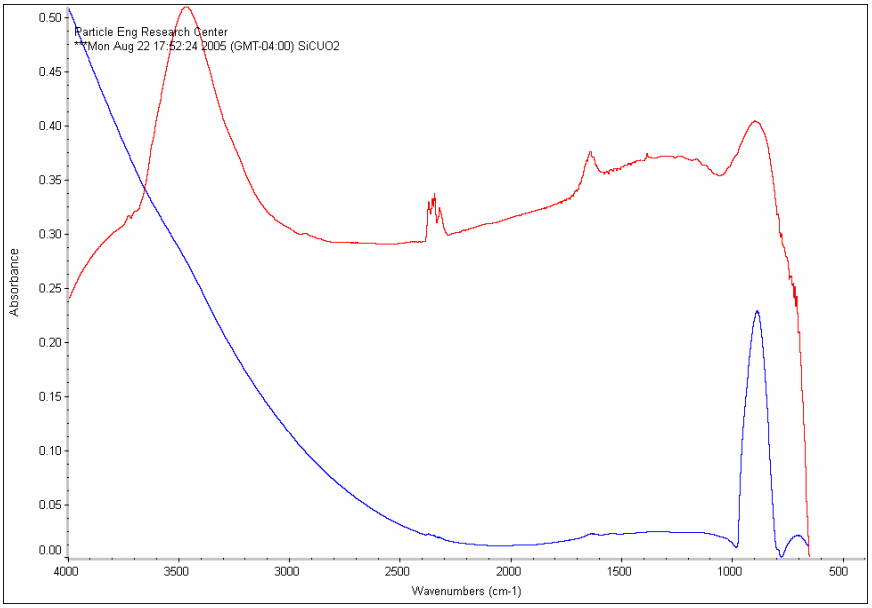

Figure 3-65. FTIR Result of $UO_{2.0}$ Powder after CVD of SiC

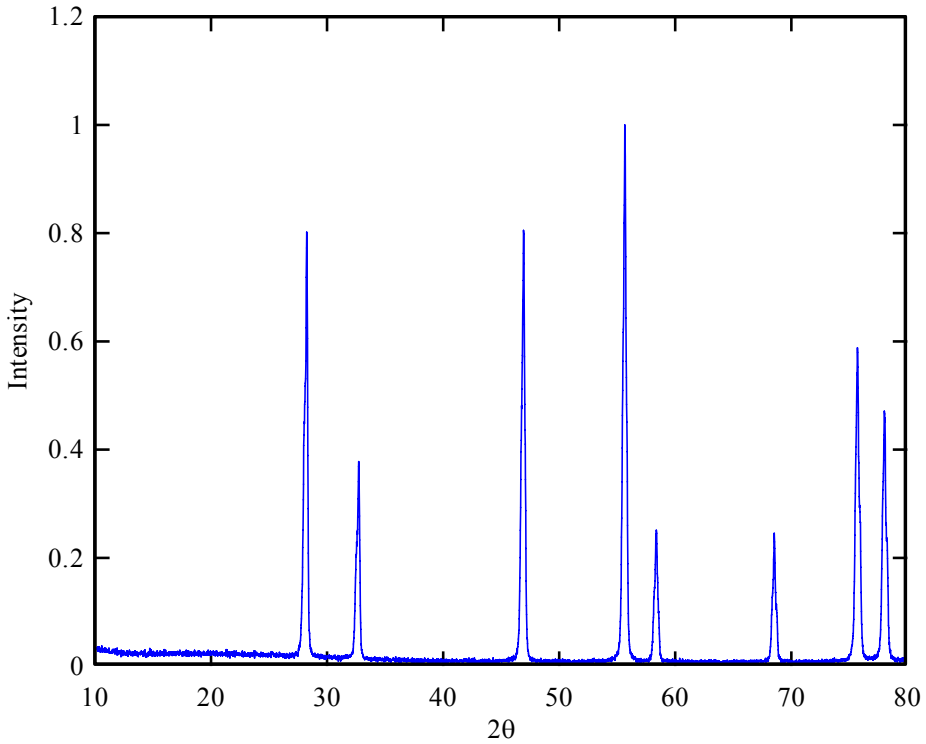

Figure 3-66. X-ray Diffraction Pattern of $UO_{2.0}$ Powder after CVD of SiC

The possible reason for the lack of success is the long furnace tube. The tube is about four feet long, and the UO_2 powder is usually placed in the middle. So the length of UO_2 powder to the opening is about two feet. Propane and TMS may already decompose at the tube wall before they reach the UO_2 powder. A colorful layer can be seen on the tube wall in Figure 3-67.

Figure 3-67. Furnace Tube after Carbonization and CVD process.

Thermal Conductivity Measurement

The thermal conductivity of the pellets is in process to be measured at the Idaho National Laboratory.

Centerline Temperature Calculation

The centerline temperature of the fuel rod in reactor can be calculated by Equation 3-8 [42]. The thermal conductivity of SiC was used for SiC-UO_2 composite assuming the formation of percolation pathway. Table 3-4 shows the centerline temperatures of the UO_2 fuel and the SiC-UO_2 composite. The centerline temperature of SiC-UO_2 composite is 700 ^oC lower than that of the UO_2 fuel, and only 300 ^oC higher than the coolant.

$$T_{cl} - T_m = \frac{q'}{2\pi r_f}\left[\frac{r_f}{2k_f} + \frac{1}{h_g} + \frac{t_c}{k_c} + \frac{r_f}{h_s(r_f + t_c)}\right]$$

Equation 3-8

Where T_{cl} is the fuel centerline temperature (K)

T_m is the moderator temperature (K)

q' is the linear power density (W/cm)

r_f is the radius of fuel pellet (cm)

k_f is the average thermal conductivity of fuel (W/(cm*K))

h_g is the gap heat transfer coefficient (0.5---1.1) (W/(cm^2*K))

k_c is the thermal conductivity of cladding (W/(cm*K)

h_s is the coefficient of convective heat transfer (2.8---4.5) (W/(cm^2*K)

t_c is the clad thickness (cm)

Table 3-4. Centerline Temperatures of UO_2 and SiC-UO_2 composite.

	Tmod (k)	q'	rf	kf	hg	kc	hs	tc	Tcl (k)
UO_2	600	263.9	0.47	0.027	0.5	0.15	2.8	0.067	1625
					1.1		4.5		1517
SiC+UO_2	600	263.9	0.47	0.550	0.5	0.15	2.8	0.067	885
					1.1		4.5		777

CHAPTER 4
DISCUSSION

To increase the thermal conductivity of uranium dioxide (UO_2), high thermal conductivity material silicon carbide (SiC) was used as an additive to UO_2. Three methods to incorporate SiC into UO_2 were studied in this research. First, silicon carbide whiskers were mixed with UO_2 particles and then hot press sintered to achieve dense pellets. Second, a polymer precursor, allylhydridopolycarbosilane (AHPCS), was used to generate a SiC coating on UO_2 particles prior to the hot press sintering process. Third, a SiC layer on UO_2 was deposited by the chemical vapor deposition (CVD) process prior to the sintering process.

Because a reaction between SiC and UO_2 occurs at 1377 ^oC, the commonly used pressure-less sintered method can not be used to fabricate SiC-UO_2 composite. A two stages low temperature sintering method for UO_2 was used to avoid the reaction. The uranium oxide powder was oxidized in air or blended with U_3O_8 to achieve an O/U ratio close to 2.30. A UO_2 pellet of 95% TD can be sintered at 1200 ^oC in inert environment, followed by 3 hours soaking in hydrogen at the same temperature to bring the O/U ratio back to 2.0. The low temperature sintering method significantly reduces the sintering temperature of UO_2, hence, reduces the energy cost and furnace maintenance cost.

Silicon carbide whiskers were used to increase the thermal conductivity of UO_2. Uranium oxide powder with extra oxygen was mixed with separated SiC whiskers and hot pressed at 1200 ^oC. Hot pressing is required to achieve a dense pellet because the whiskers interfere with the matrix particle rearrangement during sintering. The densities of sintered pellets were in the range of 94.69%TD to 99.76%TD. The scanning electron microscope (SEM) images of the pellets showed that uranium oxide powder didn't form as large a grain size as pure UO_2 pellets would, and SiC whiskers are intact within the uranium oxide matrix. However, the X-ray

diffraction pattern of sintered pellets showed no SiC peak. The probable explanation is the SiC whiskers are too small, especially the small diameter and large aspect ratio, so the X-rays diffracted by SiC whiskers are not significant compared to the X-ray diffracted by UO_2. In addition, the X-rays diffracted by the SiC whiskers can be absorbed by the UO_2 because UO_2 is a strong X-ray absorber.

The difficulty in making SiC whisker-UO_2 composite concerns the dispersion of SiC whiskers homogenously in the UO_2 matrix. When SiC whiskers and $UO_{2.27}$ were homogenized in distilled water, the SiC whiskers tend to stay on top of uranium oxide particles because uranium oxide is heavier than SiC whiskers. The mixture powder after drying must be grounded by mortar and pestle or ball milled to homogenize the SiC whiskers and uranium oxide particles.

The SiC coating on UO_2 particles was not successfully produced by polymer precursor due to the fact that the polymer precursor can be easily oxidized by the uranium oxide powder with extra oxygen. The SiC coating on UO2 particles was not successfully produced by chemical vapor deposition (CVD) due to the decomposition of gaseous precursor before it reached the UO_2 powder.

Though the thermal conductivity of sintered composite pellets has not been measured yet. The thermal conductivity of SiC whiskers-UO_2 composite to be measured by the Idaho National Laboratory is expected higher than the single phase UO_2 pellet based on the reported increase in thermal conductivity of SiC whiskers reinforced ceramic materials reported in the literature.

LIST OF REFERENCES

1. Fink, J. K. (2000). "Thermophysical properties of uranium dioxide." Journal of Nuclear Materials **279**(1): 1-18.
2. Wang, Guan-Hwa et al, U.S patent 5619433 "Real-time analysis of power plant thermohydraulic phenomena."
3. Slack, G. A. (1964). "Thermal Conductivity of Pure and Impure Silicon, Silicon Carbide, and Diamond." Journal of Applied Physics **35**(12): 3460-3466.
4. Allen, G. C., J. A. Crofts, et al. "High temperature reactions between uranium dioxide and silicon carbide." pp 630-639 of Reactivity of Solids. Anderson, J.S. (ed.). London ;Chapman and Hall Ltd., 1972.; From 7. international symposium on the reactivity of solids, Bristol, UK, 17 Jul 1972, 21 Jul 1972. See CONF-720703--. In Reactivity of Solids.
5. McEachern, R. J. and P. Taylor (1998). "Review of the oxidation of uranium dioxide at temperatures below 400°C." Journal of Nuclear Materials **254**(2-3): 87-121.
6. Loopstra, B. O. (1964). "The Crystal Structure of Trigonal U_3O_8", Acta Cryst. 17, 651-654.
7. Hobson, I. C., R. Taylor, et al. (1974). "Effect of porosity and stoichiometry on the thermal conductivity of uranium dioxide." Journal of Physics D: Applied Physics **7**(7): 1003-1015
8. http://www.nuc.berkeley.edu/thyd/ne161/mspeer/uo2fuel.html#Contents
9. Schaefer, E. A. and J. O. Hibbits (1969). "DETERMINATION OF OXYGEN TO URANIUM RATIOS IN HYPO-AND HYPERSTOICHIOMETRIC URANIUM DIOXIDE AND TUNGSTEN-URANIUM DIOXIDE." **41**(2): 254-9.
10. Lucuta, P. G., H. Matzke, et al. (1996). "Pragmatic approach to modelling thermal conductivity of irradiated UO_2 fuel: review and recommendations." Journal of Nuclear Materials **232**(2-3): 166-180
11. Samuel Glasstone, Alexander Sesonske. "Nuclear Reactor Engineering" Page 503.
12. Kim, S.-H., C.-Y. Joung, et al. (2006). "Fabrication method and thermal conductivity assessment of molybdenum-precipitated uranium dioxide pellets." Journal of Nuclear Materials **352**(1-3): 151-156.
13. Ishimoto, S., M. Hirai, et al. (1996). "Thermal conductivity of UO_2-BeO pellet." Journal of Nuclear Science and Technology **33**(2): 134-140.
14. Sarma, K. H., J. Fourcade, et al. (2006). "New processing methods to produce silicon carbide and beryllium oxide inert matrix and enhanced thermal conductivity oxide fuels." Journal of Nuclear Materials **352**(1-3): 324-333.
15. Harris, Gary L. Properties of Silicon Carbide. (pp. viii). Institution of Engineering and Technology.
16. J. A. Powell, L. G. Matus, and M. A. Kuczmarski, *J. Electrochem. Soc.*, 134, 1558 (1987).
17. H. Nagasawa and Y. Yamaguchi, *Springer Proceedings in Physics*, Vol. 71, p. 40, Springer-Verlag, Berlin (1992).
18. A. J. Steckl, C. Yuan, J. P. Li, and M. J. Loboda, *Appl. Phys. Lett.*, 63, 3347 (1993).

19. Kunstmann, T. and S. Veprek (1995). "Heteroepitaxy of **β-SiC** from methyltrichlorosilane and methyltribromosilane on Si(100) without a carbon buffer layer." Applied Physics Letters **67**(21): 3126
20. Zheng, J. and M. Akinc (2001). "Green state joining of SiC without applied pressure." Journal of the American Ceramic Society **84**(11): 2479-2483.
21. James F. Shackelfold (2000), "CRC Materials Science and Engineering Handbook". Table 91.
22. Price, R. J. (1977), "PROPERTIES OF SILICON CARBIDE FOR NUCLEAR FUEL PARTICLE COATINGS." **35**(2): 320-336
23. Price, R. J. (1973), "THERMAL CONDUCTIVITY OF NEUTRON IRRADIATED PYROLYTIC beta -SILICON CARBIDE." **46**(3): 268-272.
24. Snead, L. L. and J. C. Hay (1999), "Neutron irradiation induced amorphization of silicon carbide." Journal of Nuclear Materials **273**(2): 213-220.
25. Verrall, R. A., M. D. Vlajic, et al. (1999), "Silicon carbide as an inert-matrix for a thermal reactor fuel." Journal of Nuclear Materials 274(1-2): 54-60.
26. Hirayama, H., T. Kawakubo, et al. (1989), "Corrosion Behavior of Silicon Carbide in 290^{o}C Water." Journal of the American Ceramic Society **72**(11): 2049-2053.
27. Lippmann, W., J. Knorr, et al. (2001), "Investigation of the use of ceramic materials in innovative light water reactor - fuel rod concepts." Nuclear Engineering and Design **205**(1-2): 13-22.
28. Solomon, A. A., J. Fourcade, et al. (2004), The polymer impregnation and pyrolysis method for producing enhanced conductivity LWR fuels, Orlando, FL, United States, American Nuclear Society, La Grange Park, IL 60526, United States
29. Fuhrman, N., J. L. C. Hower, et al. (1963), "Low-temperature sintering of uranium dioxide." American Ceramic Society -- Journal **46**(3): 114-121.
30. Langrod, K. (1960), "SINTERING OF URANIUM OXIDE IN THE RANGE OF 1200-1300^{o}C." American Ceramic Society Bulletin (U.S.); Vol: 39: Pages: 366-9
31. Ayaz, B. and A. N. Bilge (2000), "Possible usage of ex-ADU uranium dioxide fuel pellets with low-temperature sintering." Journal of Nuclear Materials **280**(1): 45-50.
32. Williams, J., E. Barnes, et al. (1959), "Sintering of uranium oxides of composition UO₂ to U₃O₈ in various atmospheres." Journal of Nuclear Materials **1**(1): 28-38.
33. Wei, G. C. and P. F. Becher (1985), "DEVELOPMENT OF SiC-WHISKER-REINFORCED CERAMICS." American Ceramic Society Bulletin **64**(2): 298-304.
34. Sun, L., J.-S., Pan, et al. (2001), "An improvement in processing and fabrication of SiC-whisker-reinforced MoSi2 composites." Journal of Materials Science Letters **20**(15): 1421-1423.
35. David Belitskus, "Fiber and whisker reinforced ceramics for structural application." Page 82.
36. David Belitskus, "Fiber and whisker reinforced ceramics for structural application." Page 83.
37. R. Warren, "Ceramic-Matrix Composites." Page 247
38. Hasselman, D. P. H., K. Y. Donaldson, et al. (1996), "Thermal conductivity of vapor-liquid-solid and vapor-solid silicon carbide whisker-reinforced lithium aluminosilicate glass-ceramic composites." Journal of the American Ceramic Society **79**(3): 742-748.

39. Russell, L. M., L. F. Johnson, et al. (1987). "THERMAL CONDUCTIVITY/DIFFUSIVITY OF SILICON CARBIDE WHISKER REINFORCED MULLITE." Journal of the American Ceramic Society **70**(10): 226-229.
40. Johnson, L. F., D. P. H. Hasselman, et al. (1987). "EFFECT OF SILICON CARBIDE FIBER OR WHISKER REINFORCEMENT ON THE THERMAL DIFFUSIVITY/CONDUCTIVITY OF AN OSUMILITE GLASS-CERAMIC." Journal of the American Ceramic Society **70**(6): 135-138.
41. James J. Duderstadt et al. (1976), "Nuclear Reactor Analysis". Page 482.